運輸省港湾技術研究所

港湾技術研究所報告

REPORT OF THE PORT AND HARBOUR RESEARCH INSTITUTE

MINISTRY OF TRANSPORT

VOL. 24 NO. 3 SEPT. 1985

NAGASE, YOKOSUKA, JAPAN

港湾技術研究所報告 (REPORT OF P.H.R.I.)

第24巻　第3号 (Vol. 24, No. 3), 1985年9月 (Sept. 1985)

目　　次 (CONTENTS)

REPORT OF THE PORT AND
HARBOUR RESEARCH INSTITUTE
Vol. 24, No. 3 (Sept. 1985)

3. Development of PHRI Geotechnical Centrifuge and its Application

Masaaki TERASHI*

Synopsis

Model test of all the physical phenomena must be based upon the rational verification of similarity conditions between a model and a prototype. Unfortunately, however, gravitational force which cannot be modeled in a scaled model in earth's gravity is dominant in the behavior of soils and foundations. The significance of model testing has been very much limited. Use of geotechnical centrifuge in the model study reduces this limitation.

A large scale centrifuge was installed in the Port & Harbour Research Institute (PHRI), Ministry of Transport, for geotechnical studies in the March of 1980. Ancillary equipments including various data acquisition system, photo-instrumentation system, loading equipments, and etc. were completed in the following two years. This is the largest centrifuge among eight geotechnical centrifuges existing in Japan. In the present articlcle, outline of the similitude of geotechnical modeling, details of the PHRI centrifuge, current research projects, and scope of the future studies are described.

* Chief of Soil Stabilization Laboratory, Soils Division

港湾技術研究所報告
第24巻 第3号 (1985. 9)

3. 遠心力載荷装置の開発とその適用

寺師 昌明*

要 旨

土の模型実験では，地盤の挙動を考える際に無視しえない自重の効果を再現できないため，その成果が極めて制限された価値しか持ちえなかった。近年，注目を集めている遠心載荷実験手法は模型を大加速度の場に置くことで，この制約のほとんどを解消するものである。

港研では港湾の分野の技術開発を促進するために，昭和50年から7年の期間をかけて，搭載質量2.7t，常用最大加速度115gの世界最大級の遠心力載荷装置を設計・製作して以来，3年間本格的に広範なテーマについて実験研究を実施してきた。

本報告では，遠心場の実験の相似則，港研の装置ならびに周辺機器（電気的・光学的計測機器）の紹介と，現在までの研究の成果の概要を示す形で，確立されてきた実験手法を紹介する。

* 土質部 地盤改良研究室長

CONTENTS

1. Introduction

Japan is quite mountainous and consists of a number of small islands. Limited spaces of plane lands in her coastal area were highly developed for many decades, which has obliged Japan to reclaim the sea seeking the site for industrial and public usage. This situation will also be unchanged in the future. For large civil engineering projects such as port or airport constructions, possible sites tend to be in the deeper sea and sub-soil conditions be more and more difficult than ever. An example for this is a project of a new international airport just started in Osaka Bay. Feasibility study for the project is suggesting that the site is at water depth of around 20 m and the soil condition is thick alluvial clay underlain by multiple layers of clay and sand of diluvial age, which appear alternatively up to 400 m from the sea bottom, according to the available data. This multiple layers of clay and sand are said to extend up to 1000 m or more. There an artificial island whose final approximate size is 5 km by 3 km is scheduled to be constructed within eight years. Major concerns there are naturally how to secure the permanent stability of the revetment and how to reduce the residual settlement.

On the contrary to such a big project, in the construction or renovation of local ports, the conventional design concept of structures free from maintenance has to be abandoned in some cases, because such a concept may lead to high construction cost and budget allocation becomes difficult owing to the recent severe budget deficit. It means that an alternative design concept of construction must be established which allows relatively large residual settlement but reduces the initial construction cost considerably with the expense of future maintenance works.

In either case, the design codes for port construction available today must be reviewed and renewed. Also the development of new construction techniques is required. These are the task for the research group at the Port & Harbour Research Institute. Both ideas of new designs and new techniques which will come out must be verified by some means. Sophisticated techniques of numerical and/or physical simulation of the behavior of earth and structure are required. The PHRI geotechnical centrifuge has thus been planned and facilitated in the Institute. Centrifuge itself has been installed in the March of 1980 and surrounding facilities, e. g., electrical and photographic data acquisition system and loading equipments, have been provided by 1982.

In the present article, outline of the similitude of geotechnical modeling, details of the PHRI centrifuge, current research projects, and scope of the future studies are described.

2. Significance of Centrifuge Modeling in Geotechnical Studies

2.1 Necessity of Modeling

Civil engineers are responsible for the safe and economical construction and satisfactory performance of huge structures. To achieve this task, rigorous prediction of the behavior of structure during its expected life must be carried out with sufficient accuracy by means of theoretical, numerical, empirical, or experimental approach. In the actual work, engineers choose suitable procedures of prediction among various alternatives usually from the manual or codes of design. Ordinarily, these means are described in the form of theoretical formula, tables or design diagrams. However, such procedures are always based on the simplified assumptions and hence are valid only within the validity of the assumptions.

The simplified Bishop method of slip circle analysis of slope stability, for example,

is based mainly on the following assumptions ; i. e. the soil in concern is assumed to be rigid plastic material having the failure criterion of usually a Mohr-Coulomb type, and the failure surface to be circular. These assumptions are undoubtedly insufficient in the light of recent soil mechanics. Furthermore, the calculation ignores the fundamental equilibrium of horizontal forces. However, this technique is widely accepted for the stability analysis as long as the slope in concern is composed of ordinary soil material and the method is utilized with appropriate shear strength of the soil under a suitable factor of safety. This is not because the method is entirely correct but because the method is convenient for a routine design and the accuracy of the method is verified by a number of unfortunate failures of the slopes. Therefore, when one wants to utilize a certain design technique, he must have a clear understanding of the assumptions adopted for the derivation of the technique and he must use the technique within the range of its validity.

When one feels that the accuracy of an existing approach is insufficient but still prefers to utilize the technique, he wants to adjust the calculation by some means. One example is the prediction of consolidation settlement and the prediction of the time required to reach a certain degree of consolidation. Terzaghi's classic consolidation theory is often utilized for that purpose. The necessary soil properties for the calculation are obtained by the oedometer test, which is a scaled model test of consolidation phenomenon. But as is well known, the method is practical only when the settlement is small and the structure in concern is thought to be one dimensional. Therefore, it is a routine practice for a designer to adjust the calculation by the observed settlement-time or pore pressure-time relationship. This is a typical example of full scale model test at the same site using the very structure of concern, but this is one of the very rare examples where he can conduct a full scale model testing.

When one encounters an entirely new problem, new structure or familiar structure but beyond the previous experiences, he must try to check the validity of the existing technique by himself. In that case, the best way is to observe the behavior of the actual structure and check the accuracy of the existing procedure or establish a new design technique abstracting new assumptions from the observation of full scale structure. However, the full scale test to observe the behavior of an actual structure is almost always very costly, takes a long time, and sometimes is very dangerous. Furthermore, it is almost impossible to carry out a parametric study and to check the reproducibility of the test results. There the necessity of scaled modeling arises to replace full scale observations.

2.2 Consideration on Similarity Condition

In order to predict the prototype behavior correctly from the observation of model behavior, similarity condition must be established for the model and the prototype. Similarity condition is derived by one of the following ways.

i) List up all the physical quantities that characterize the phenomenon in concern. Using Buckingham's theory, establish dimensionless numbers as the product of above physical quantities. Finally, equate the dimensionless numbers between the model and the prototype to obtain the scaling factor for each quantity.

ii) List up the physical principles (or laws) that are considered to govern the phenomenon in concern. Derive dimensionless numbers from the principles and equate them between the model and the prototype.

iii) Derive the dimensionless numbers from the differential equations that govern the phenomenon and equate them between the model and the prototype, if the equations are known.

Among these procedures, i) is the most fundamental way leading to similarity.

However, the selection of physical quantities is not always easy. Therefore, with increasing knowledge on the phenomenon, ii) or iii) is preferred.

The importance of the similarity between the model and the prototype is well described by Rocha (1957) and Roscoe (1967) as follows. Rocha considered the important forces acting on a saturated soil element whose surface area is S and volume V. The forces acting on the solid phase of the element is shown in Fig. 1 a) and those on the fluid phase is shown in Fig. 1 b).

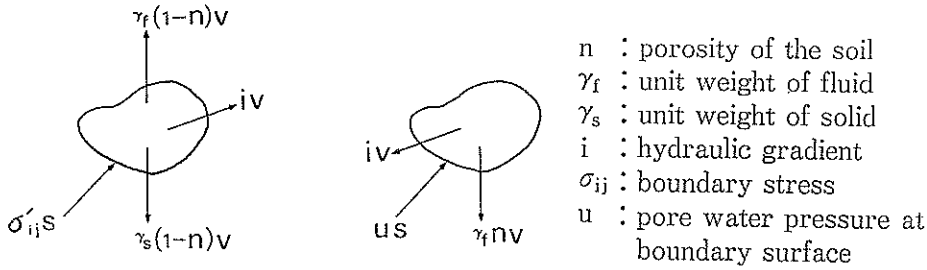

a) Solid phase b) Fluid phase

Fig. 1 Forces Acting on a Small Element of Soil

Then Rocha compared those forces between the model and the prototype where the linear scale ratio is h (h=length$_p$/length$_m$). Hereafter, the subscripts p and m refer to the prototype and the model, respectively. He made two assumptions; one for the material properties and the other for fluid flow within the soil element. Each material has a similar unique stress-strain relation (Fig. 2) independent of time where $\sigma_p/\sigma_m=\alpha$ and $\varepsilon_p/\varepsilon_m=\beta$. Fluid flow is assumed to obey well known Darcy's law $q=ki$, where q is the volume of fluid flowing per unit time per unit area, k is the permeability and i is the hydraulic gradient.

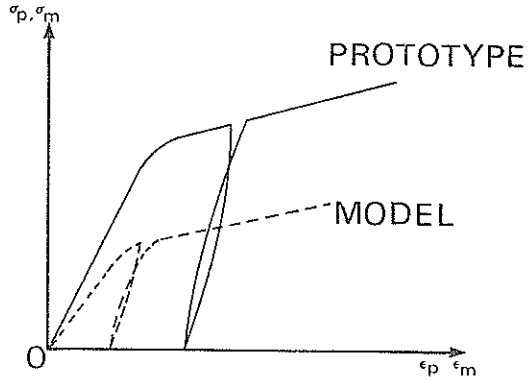

Fig. 2 Stress Strain Relation of the Material

After some calculations, similarity conditions become as follows;

$$n_m=n_p \tag{1}$$

$$\rho=\gamma_{sp}/\gamma_{sm}=\gamma_{fp}/\gamma_{fm} \tag{2}$$

$$\alpha = h\ \rho \tag{3}$$

$$k_p/k_m = (h^2\ \beta)/(\alpha\ t) \tag{4}$$

where t is a scaling ratio for time; $t = t_p/t_m$.

The difficulty to satisfy all these similarity conditions for the ordinary soil mechanics problems might be soon understood. The most important condition is the third one, which restricts the experiment to be carried out under the condition of $\alpha \fallingdotseq h$ practically. The ordinary model scale is 1/50−1/100 and hence the strength of the model must be very small. This difficulty will not arise only if the body force is insignificant in the phenomenon of the soil in comparison with the boundary stresses. However, unfortunately, this is not the case in the ordinary soil's problem.

2.3 Similarity in Geotechnical Centrifuge Modeling

The difficulty in the modeling discussed in the previous section comes from the evidence that one cannot change the unit weight of soil-like material dramatically as long as both the model and the prototype are placed in the same gravitational field. Considering that the unit weight γ is a product of the density m and the acceleration a, the equation (3) is rewritten as follows;

$$\alpha = (m_p\ a_p/m_m\ a_m)\ h \tag{5}$$

The gravitational acceleration on the earth a_p is always unity. However, if one can arbitrarily choose the gravitational acceleration on the model a_m, then the most difficult restriction on the model testing will disappear. When the same material is used both in the model and the prototype, $\alpha = 1$ and $m_p = m_m$ and consequently $a_m = a_p h$ satisfies the similarity condition.

The idea of applying centrifugal acceleration to model testing was said to be originally proposed by French engineer Phillips in 1869. The idea was put into practice by Bucky in 1931 in USA and by Pokrovsky and Davidenkov at around the same time in USSR. Since then, centrifuge modeling seems to have been conducted continuously in USSR (Yakovleva, 1985). However in the western world, there has been a very limited number of studies carried out since that time. The recent geotechnical centrifuge study has been initiated in the middle of 1960's by Schofield in UK and Mikasa in Japan (Avgherinos and Schofield, 1969, Mikasa et al., 1969).

The similarity for the centrifuge modeling has been well established by many workers and summarized, for example, by Ovesen in his report on the state of the art (Ovesen, 1985). Generally in the centrifuge model test, centrifugal acceleration N times greater

Table 1 Scaling Relationships

Physical Quantity	Prototype at 1 g : Model at N g
Length	1 : $1/N$
Acceleration	1 : N
Mass	1 : 1
Force	1 : $1/N^3$
Stress	1 : 1
Strain	1 : 1
Displacement	1 : $1/N$
Time laminar flow	1 : $1/N^2$
inertia	1 : $1/N$
creep	1 : 1

than the earth's gravitational acceleration is applied to $1/N$ scaled model. Scaling relationships for various physical quantities are listed in Table 1, where the model material is the same material as that of prototype.

As is already understood, the centrifuge modeling technique is far superior to the scaled model test in the 1 g field. One can rely on the centrifuge model test results not only qualitatively but also quantitatively. However, still one has to pay attention to two contradictions ; one is the scaling ratio of soil grain size and the other is the different time scaling ratio for different events. When the same material is used in the model and prototype, the scaling ratio for the grain size is unity. Therefore, in this regard, one has to check the magnitude of distortion of the test results due to grain size or by other source of distortion by changing the acceleration in simulating the same hypothetical prototype, which is called modeling of the model. In the regard of time scale, one must consider the most significant phenomenon in his model.

Ovesen (1985) states : *In modeling it is essential to recognize the following three fundamentals* :

—*All significant influences should be modeled in similarity,*

—*All effects not modeled in similarity should be proven secondary by experimental evidence, and*

—*Any unknown effect should be revealed or proven insignificant by means of the test results.*

3. PHRI Geotechnical Centrifuge

3.1 Determination of the Capacity

As is already described in the previous chapter, one can reproduce the prototype stress condition by simply applying N g to $1/N$ scaled model. And the scaling relationships for various physical quantities become those listed in the Table 1. However it does not mean that a centrifuge modeling under any arbitrary g level can always produce a reliable model test results. One can probably rely on a very small model under very high acceleration as long as one tries to model geometrically simple prototype behavior with little influence of water migration. If one tries to simulate a behavior in multiple layered ground or a behavior of pile foundation for example under 1000 g, a layer of one meter thickness and a pile of one meter in diameter must be simulated by one millimeter in the 1/1000 scaled model which is practically impossible. Modeling of an undrained behavior under 1000 g is inpracticable, because one minute in the model becomes equivalent to 2 years in the prototype life. If one considers the instrumentation, even the miniature transducer with the diameter of 5 mm becomes as big as 5 m under 1000 g and disturbs the model soil condition. Furthermore, transducers must endure such a high acceleration.

Therefore, in the determination of the capacity of centrifuge, one has to understand the influence of various specifications of the centrifuge to the modeling of prototype.

1) Effective radius of the centrifuge :

In the prototype, the acceleration field is practically parallel and the magnitude of acceleration is practically uniform, while, in a centrifuged model ground the acceleration field is radial and the magnitude is proportional to radius. Therefore, if the effective radius which is a radius of a point of major concern in the model ground is small, variation of the acceleration within the model becomes large and the stress field in the geometrically similar model should be distorted. Avgherinos and schofield (1969) suggested that if the model height is kept less than one tenth of the radius, the variation in acceleration will be less than $\pm$ 5 %.

2) Maximum payload and maximum acceleration :

The maximum payload naturally gives the upper limit to the total weight of the model ground, strong box to contain the model, surrounding equipment for simulating the construction procedure or external forces, and instrumentation etc. It means that the maximum payload gives the restriction on the size of actual model. The size of the model multiplied by the maximun acceleration gives one the idea of the maximum extent of prototype which can be modeled in a particular centrifuge. This is why the capacity of centrifuges are compared usually by the product of maximum payload and maximum acceleration expressed in g-tons. However, as is already mentioned above, extremely high g gives one a lot of trouble in modeling the prototype.

Therefore, the longer the effective radius and the larger the maximum payload, the better is the quality of models. At the same time, however, the cost for construction, maintenance, and experiment increases exponentially with increasing scale of the centrifuge. Up to the present, the working acceleration from 50 g to somewhere around 100 - 150 g are preferred in the centrifuge world. Other specifications of the centrifuge may be determined by the expected scale of prototype and of course by the available budget.

Based on these considerations, the effective radius of the PHRI centrefuge was determined as around 3.5 m and the working acceleration as around 100 g. For the prototype structure in port and harbor area, a reasonable soil area to be modeled is consideted to be 150 m × 150 m in plan. Therefore, the minimum space of the swinging platform required was 1.5 m × 1.5 m on which the specimen container should be mounted. At this moment, PHRI centrifuge is the largest active geotechnical centrifuge in Japan as shown in Table 2 and one of the largest in the world.

Table 2 Major Specifications of Geotechnical Centrifuges in Japan

	Osaka City Univ.	Tokyo Inst. of Tech.	Public Works Res. Inst.	Chuo Univ.	Toyo Const.	PHRI
Max. Effective Radius (mm)	2,560	1,250	1,250	1,180	2,200	3,800
Max. Accerelation (g)	200	150	360	270	250	115
Max. Payload (kg)	200	250	130	150	300	2,710
Max. Capacity (g-tons)	40	38	40	30	75	300

3.2 General Arrangements of the Centrifuge

The main part of the centrifuge is housed in the underground reinforced concrete pit for the safe operation. The inner size of the pit is 10.4 m in diameter and 4.2 m in height. As the soft rock appears at the depth of 3.5 m at the site, the bottom of the pit is buried in the soft rock.

Main part of the centrifuge weighs approximately 60 tons and whose diameter is 9.5m (Fig. 3 & 4). Two swinging platforms are hinged to the rotating arm via the torsion bar systems to safely deliver the radial force at high acceleration to the end plates at both ends of the arm (Fig. 5 & 6).

The drive unit for the centrifuge (400 kW direct current motor) is mounted on the upper floor of the pit (Fig. 7) and generates steady acceleration up to 115 g (115 times as large as earth's gravity) at the surface of the platform whose radius during flight is 3.8 m. Effective working radius for a model is around 3.5 m because specimen container

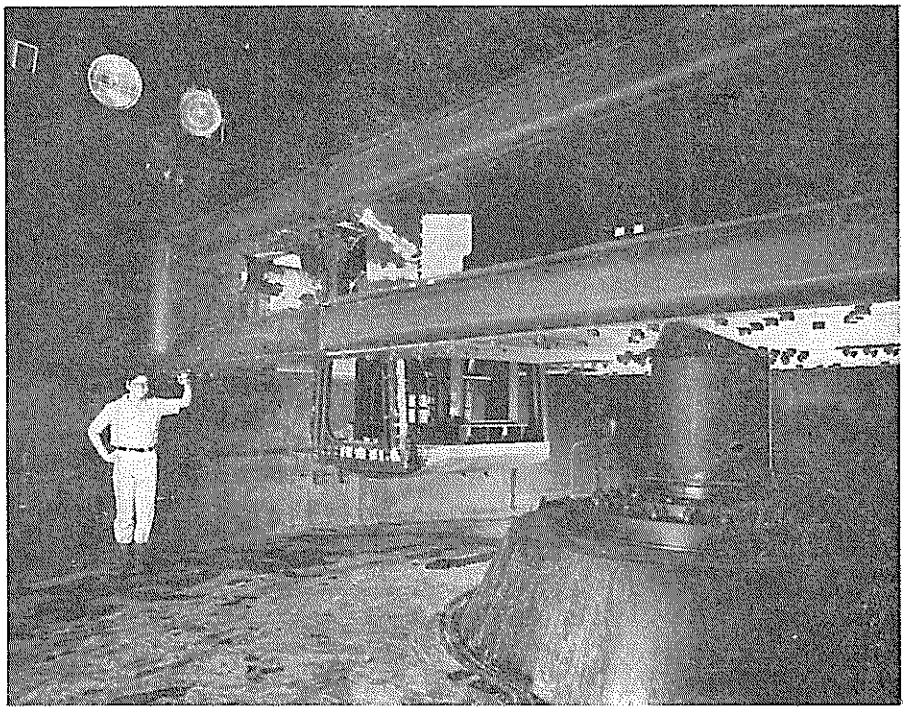

Fig. 3 Photograph of PHRI Centrifuge

Table 3 Major Specifications of PHRI Centrifuge

Maximum acceleration (g)	115
Diameter of rotating arm (mm)	9, 650
Maximum effective radius (mm)	3, 800
Maximum Number of rotation (rpm)	165
Space of swinging platform (mm)	1, 600×1, 600
Maximum payload (kg)	2, 710
Maximum capacity (g-tons)	300
Main motor (kW)	400
Electric slip ring (poles)	80
Rotary transformer (kVA)	5. 2
Number of hydraulic joints	10
Total weight of the centrifuge (tf)	87

(strong box) is mounted on the platform.

Two dimensional plane strain test is usually carried out in the very strong box which will not allow a change of strain perpendicular to the plane. And in such a test, strong box with one transparent side is preferred for the convenience of the observation of model behavior. In the case of ordinary centrifuge, the strong box lies on a horizontal plane during flight with the transparent side faced upward (horizontal setting). Hence the centrifugal component of acceleration in a model ground become radially outward. When a strong box lies on the vertical plane during flight (vertical setting), transparent

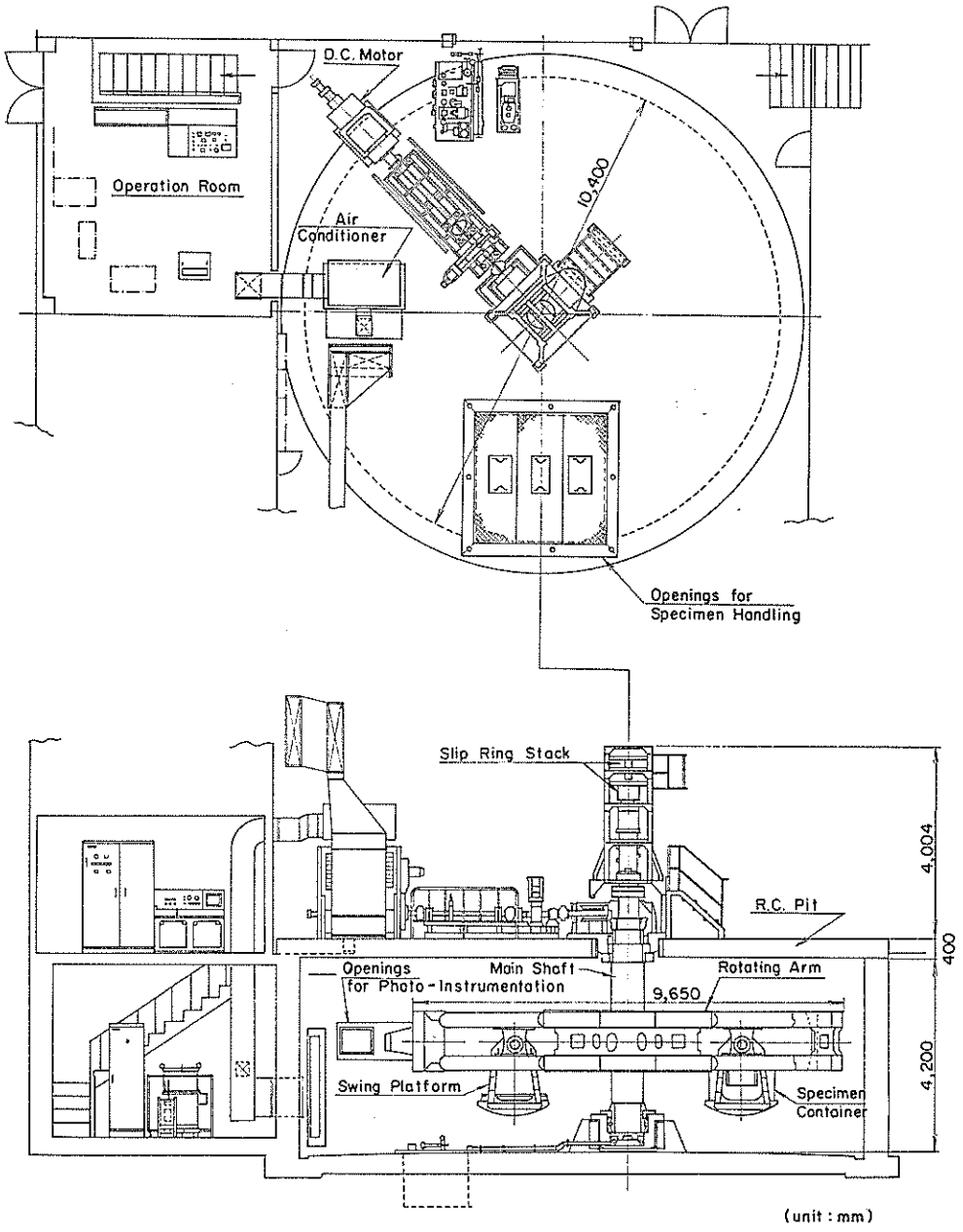

Fig. 4 PHRI Geotechnical Centrifuge

side faces toward the tangential direction of rotation. Then centrifugal acceleration becomes practically parallel in a model ground. With the PHRI centrifuge, horizontal or vertical setting of a strong box is arbitrarily chosen. The vertical setting of the specimen container became possible due to the sufficiently large space of the platform and the capability of photo-instrumentation system for both horizontal and vertical settings. For the vertical setting, photo-instrumentation and TV monitoring are carried out

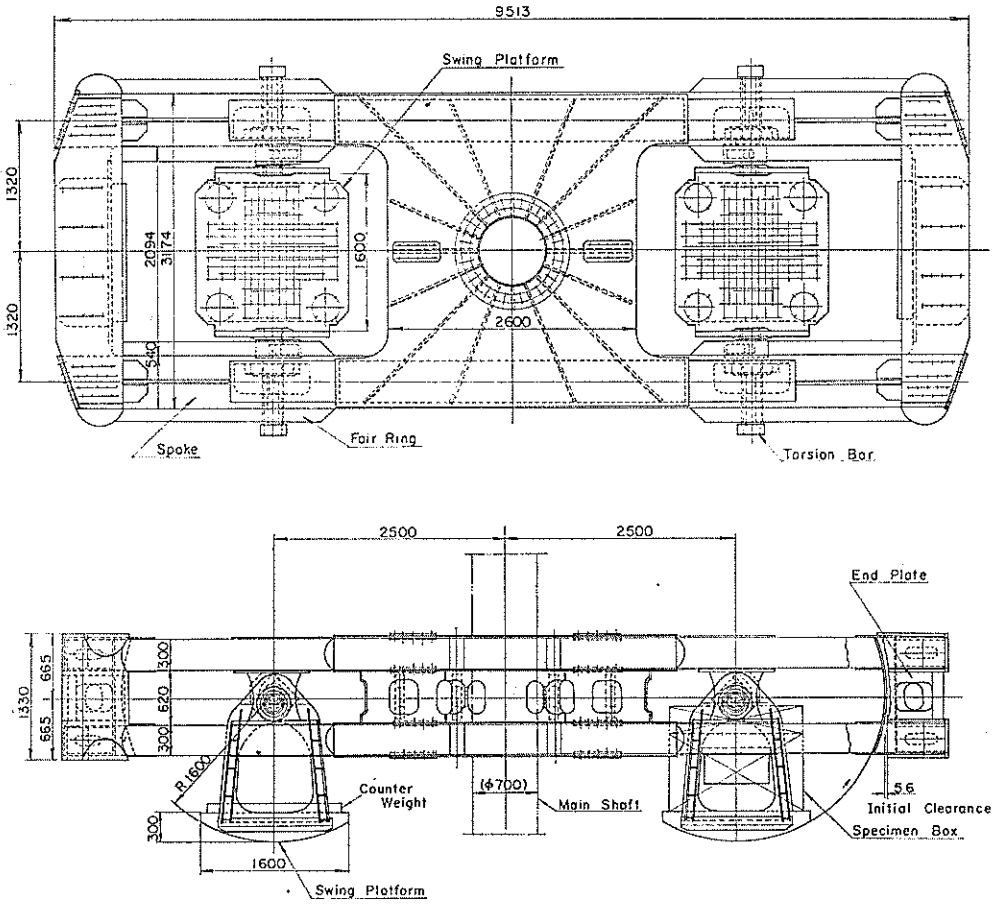

Fig. 5 Rotating Arm and Swinging Platforms

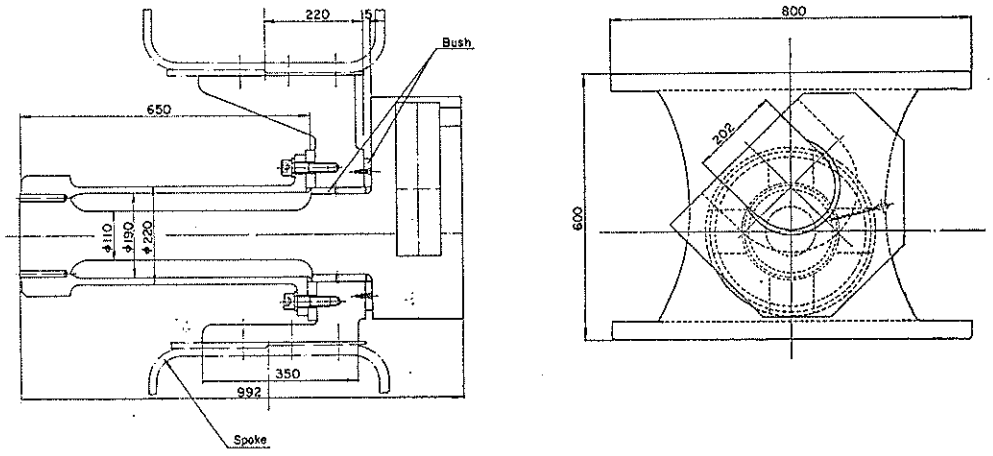

Fig. 6 Details of Torsion Bar System

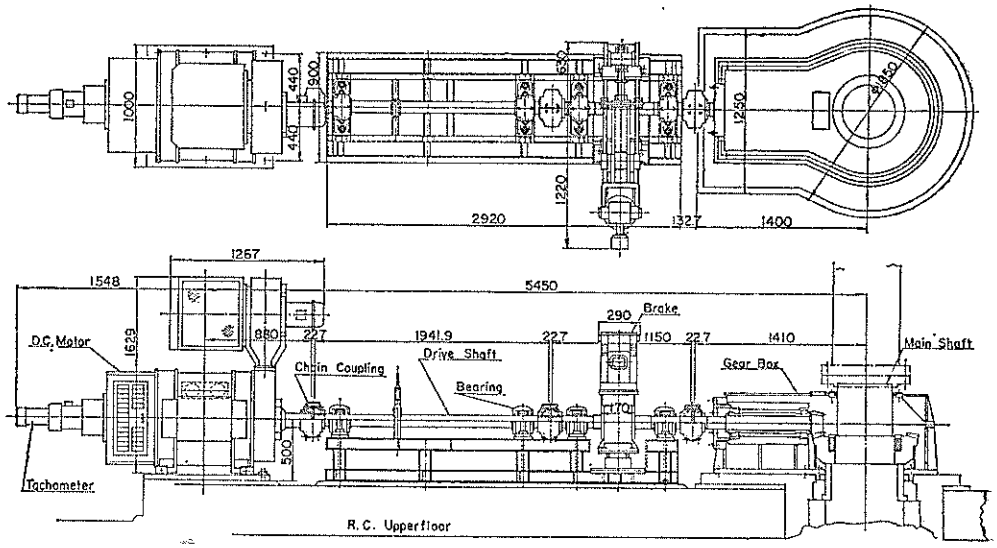

Fig. 7 Drive Unit

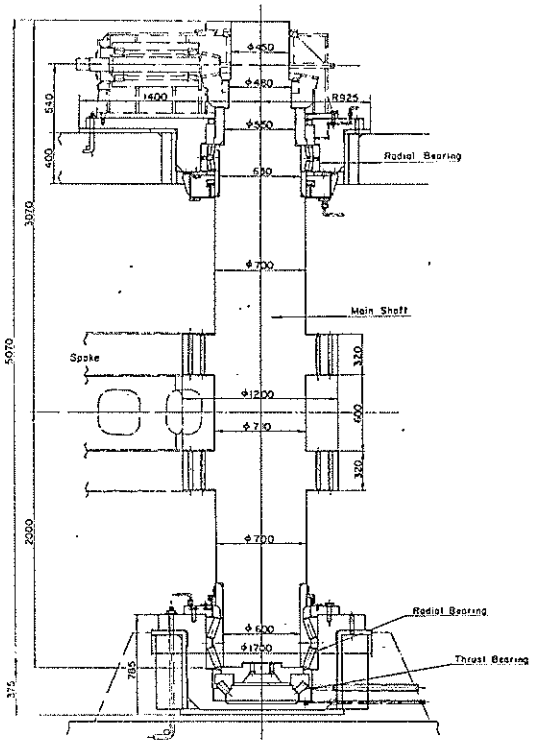

Fig. 8 Main Shaft and Bearings

through the openings of the side wall of the pit.

The control of the centrifuge is carried out in the operation room. Conditions of all the important components of the centrifuge, such as radial and thrust bearing of the

main shaft (Fig. 8), electric currents, air conditioner, lubrication, and etc. are always monitored and displayed on the control panel. Safety function is equipped to ring the alarm in the case of trivial troubles and to stop the machine automatically in the case of severe trouble.

Major specifications of the PHRI centrifuge is listed in the Table 3.

3.3 Ancillary Equipments.

Various tools and equipments to conduct the experiment in the high g field are available, such as loading devices for bearing capacity study, sand hopper for embankment

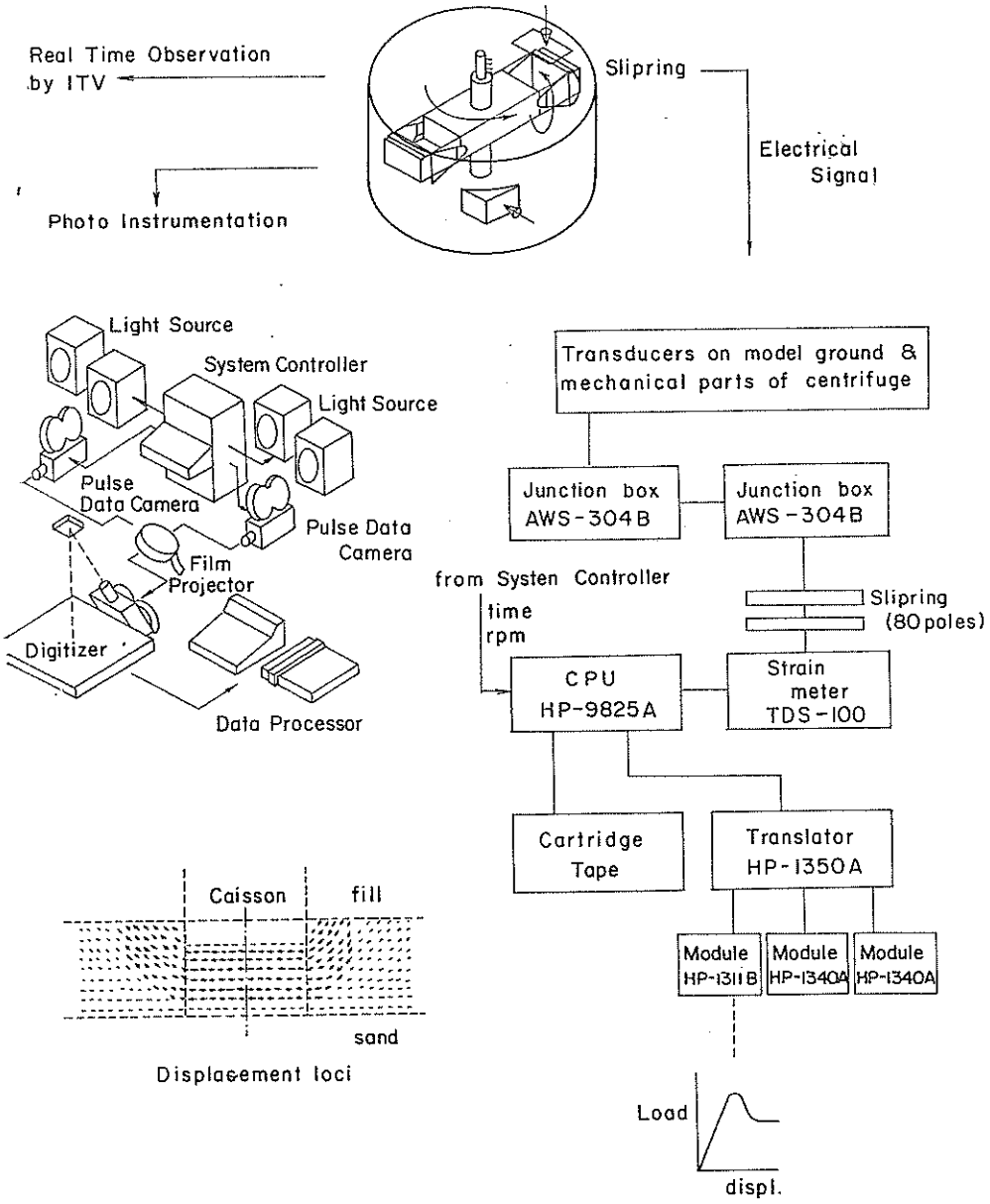

Fig. 9 Data Acquisition System

construction, vane tester and cone penetrometer for measuring in-situ (in-flight) strength of the model. In order to drive these equipments during flight, electricity (3 ϕ 200 V, 2 ϕ 100 V, DC 6−24 V) and hydraulic pressure are supplied to the platform through rotary transformer and hydraulic joints equipped at the upper part of main shaft.

Measurement of phenomena in the model ground during flight is carried out by various means, e. g., electrical measuring devices, photo-instrumentation as shown in Fig. 9.

Electric signals obtained by various transducers and the signals to control the above mentioned equipments are transmitted through a slip ring stack (80 poles) on the top of the main shaft from the swinging platform to the operation room. The analog signals from transducers are measured and converted to digital signals by the strain meter, inputten to a microcomputer, stored in the cartridge tape, and displayed on the CRT after some calculations.

Although the electric transducers give the very precise information of the phenomenon, too much instrumentation on the small model disturb the model condition and should be avoided. In the case of plane strain model tests, still photographs are very helpful in obtaining rich information. A new photographic instrumentation system has been developed for the centrifuge. The system consists of two 70 mm format pulse data cameras with 1000 ft film magazine, two high intensity short duration flash units, a sequence control unit, a film projector, a screen digitizer and a data processor.

Photographs of a model ground are taken during flight through the transparent window of the strong box (Fig. 10). Photographs can be obtained from two directions which correspond to vertical or horizontal setting mentioned previously. The coordinates of the targets on a model are then read and digitized on a large screen and compensated for various sources of distortion using fiducial points on the strong box. To increase the quality of photographic image, every optical part of the system is specially designed.

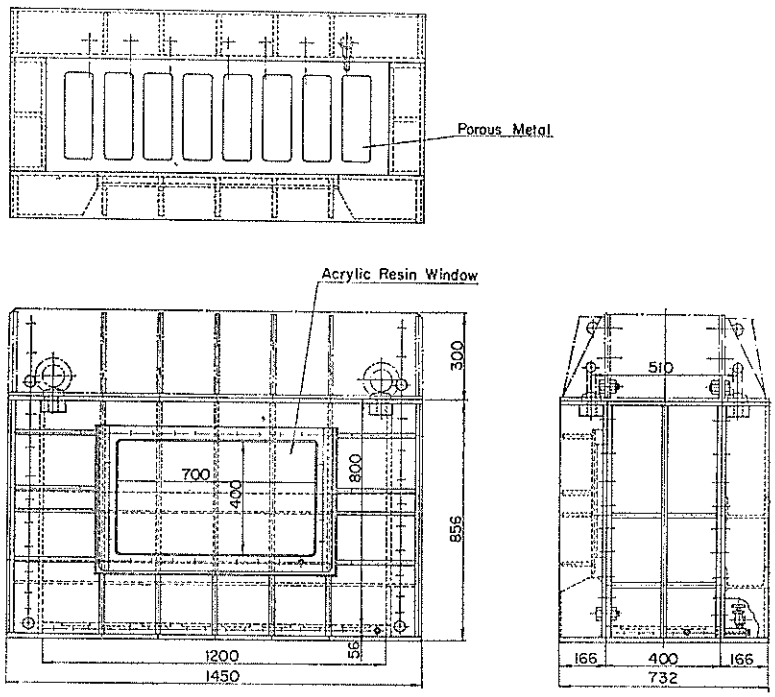

Fig. 10 Strong Box with a Transparent Side

With this system, the total accuracy of coordinates obtained by photograph is within ± 0.1 mm (Terashi, et al, 1983 a). Details of the photographic instrumentation system is described in the appendix.

A TV monitoring system is also added to the system, which is quite powerful in real time observation and quick playback although the image quality is inferior to the still photograph. The same light source with that for still photograph is used for TV monitoring. The light flashes for 30 microseconds only intermittently when the flying object passes in front of the camera. Therefore the TV camera is used with the aid of a frame memory to obtain a continuous image.

4. Current Research Projects and Scope of the Future Studies

Model studies using geotechnical centrifuge can be divided into two categories. One is the simulation of soil and structure in realistic scale to reveal unknown behaviors or to verify analytical or numerical estimation. The other is the direct simulation of the prototype existing somewhere or to be built in a future. Centrifugal modeling is particularly powerful in the former case, and the preceding research works carried out by the different organizations mostly fall into this category. However our institute belongs to the government and strong needs exist for the research to assist the design, construction and maintenance of actual structures. Therefore, the simulation of the site specific prototype is also required.

4.1 Behavior of the Improved Ground by DMM

As is mentioned in the introduction, we have to construct port facilities of increasing scale on difficult soil conditions. It is absolutely necessary to improve the soft soils in advance to the construction of the important structures. However, in some cases sufficient improvement is not possible by the conventional soil improvement techniques such as replacement or vertical drain method. The Deep Mixing Method (DMM), a kind of deep in-situ admixture stabilization has been developed originally in the Port & Harbour Research Institute to reinforce soft soils.

A DM machine is used to treat soft soils in-situ, which basically consists of several mixing blades and stabilizer supplying system. By one operation of the machine it is possible to manufacture a treated soil column whose cross sectional area ranging from 1.5 m^2 to 9.5 m^2 and length up to 40 m depending on machine type. In most of the soil improvement work for heavy structures, treated soil columns are overlapped to make a continuous treated soil mass. Details of DMM have been reported by Okumura & Terashi (1975), Terashi et al. (1979), Terashi & Tanaka (1981/1983), Kawasaki et al. (1981/1983) and Terashi et al. (1983 b).

Treated Japanese marine clays by DMM have high unconfined compressive strength of the order of 1 MN/m^2, small strain at failure of the order of 0.1 %, relatively low tensile strength, and low permeability. However, strengths of treated soils have a large deviation from its average value even if the manufacturing works were carried out with best possible care. Therefore, a sufficiently high factor of safety is taken for the strength of in-situ treated soils, which in turn results in extraordinary difference of engineering characteristics between treated and untreated surrounding soft soils. Hence, treated soil mass is considered to behave as a rigid structure buried in the soft ground.

In the current design procedure as shown in Fig. 11, external stability of the rigid buried structure is examined first to determine the extent of improvement and then internal stability of treated mass is examined by elastic analysis to keep the stresses to be lower than allowable strength of treated soil.

The Deep Mixing Method was put into practice first in 1971 and has already been

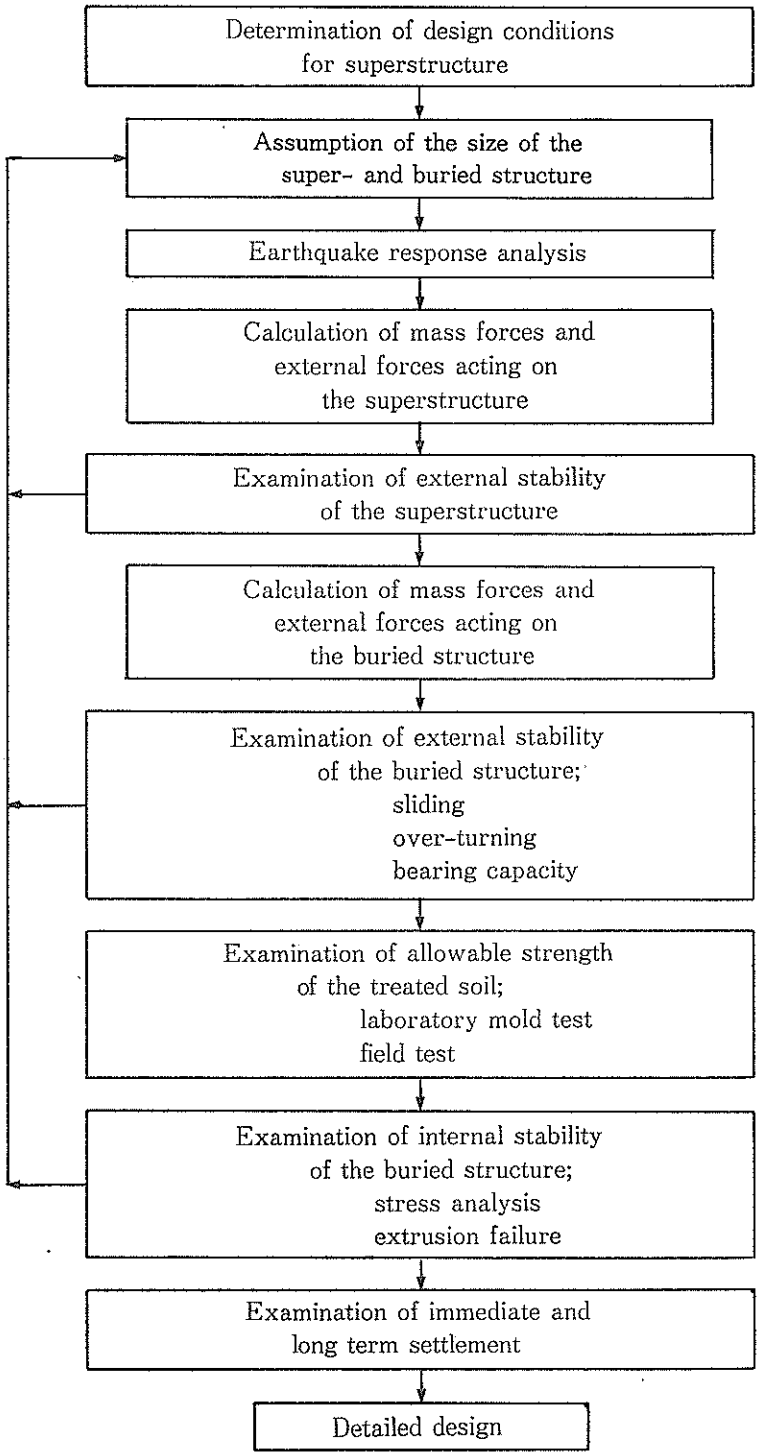

Fig. 11 Flow of Design Procedure

applied to improve soft foundation soils of several port facilities and of a number of light weight or temporary structures. Net volume of improved soil by the method has already exceeded six million cubic meters. However DMM is still a new technique in which various problems are left to be studied. For example, boring technique to obtain an undisturbed sample of stiff treated soils is still immature. A variety in DM machines results in the difference of the quality of treated soils. These problems are indirectly but closely related to the design of an improved ground.

Regarding the current design concept and procedure, much has been left to be studied to increase the accuracy of estimation and to reduce the cost of improvement. Research efforts by various organizations in Japan are concentrated to the point. At the same time, a complicated three dimensional shape of improved soil mass has been conceived of in order to minimize the volume of treated soil mass as shown in Fig. 12.

The author has started a series of research projects to reveal the behavior of the improved ground. In the initial phase of the study, each mode of failure assumed in the current design procedure is examined through pursuing the real behavior of stiff treated soil mass in the untreated ground both by numerical and physical simulation. The latter is carried out by a large scale site experiment and a series of centrifuge modeling.

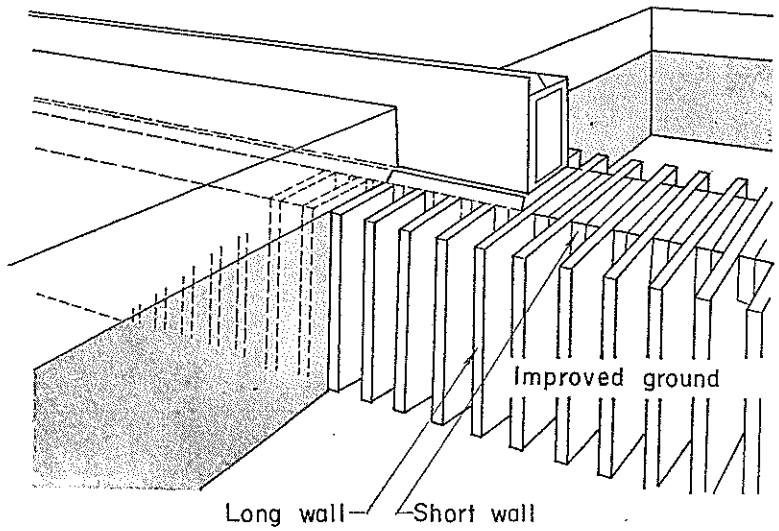

Fig. 12 Improved Ground of Wall Type

(1) Extrusion Failure

A typical failure mode for wall type is an extrusion failure in which untreated soil between the treated soil walls is squeezed out due to the unbalance of active and passive earth pressures. A total of 11 model grounds have been prepared for the test series and brought to failure by increasing the acceleration. Model ground is schematically shown in Fig. 13, where the size of the wall W_s, W_1 and the undrained shear strength of the clay Cu are varied for each test.

Models were designed to restrict a mode of failure exclusively to extrusion. Deformation of the model ground with increasing g level was measured and shown in the Fig. 14 with the points of measurement. Heave of the soft clay in front of the improved ground and settlement of the sand fill clearly show the existence of extrusion failure. Displacement and gravity are plotted on log/log scale and the acceleration at clear bend in the curve

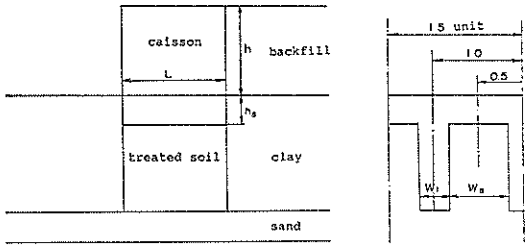

Fig. 13 Model of Wall and Untreated Soil

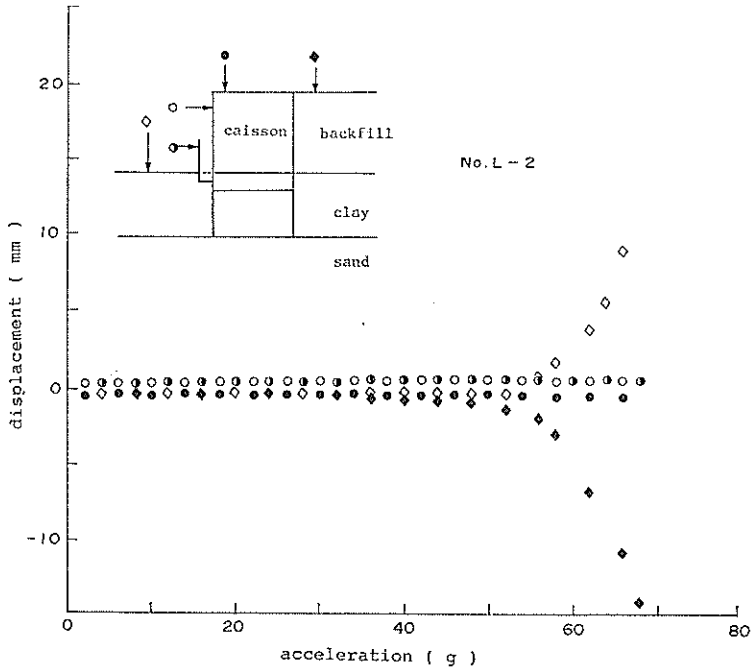

Fig. 14 Displacement vs Gravity

is defined as the acceleration at failure g_f. Using the still photographs taken during flight, the coordinates of the targets on the surface of untreated soils between the treated soil walls are measured and displacement loci are obtained as shown in Fig. 15. Seemingly, displacement loci thus obtained are parts of arcs centered at the same point on the center line of the improved ground. Shear strains developed in soft soil between the walls are calculated also from the displacements of targets considering one square grid of target as an isoparametric element (Fig. 16). The factor of safety is defined as a ratio of acceleration at failure and that at certain stage, g_f to g. This strain distribution suggests that the soft soil between the treated soil walls is squeezed out while keeping the original shape. Based on these observations, authors assumed a simple cylindrical slip surface for calculating the stability against extrusion. A kind of stability number Heq $(=\rho\, g_f h/Cu)$ obtained by the calculation and that by the centrifuge tests are in good accordance as shown in Fig. 17 (Terashi et al. 1983 b) where $\rho\, g_f h$ denotes the backfill pressure at failure.

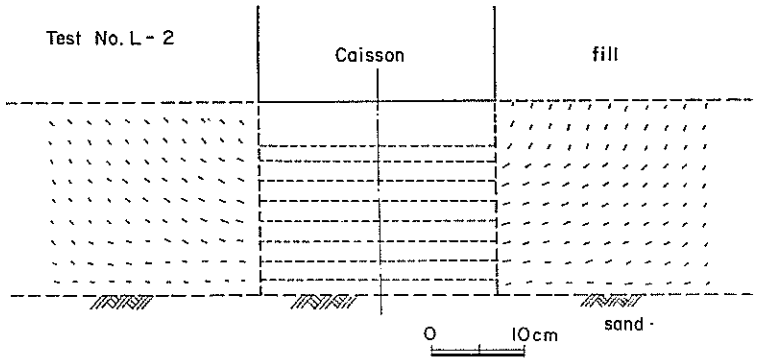

Fig. 15 Displacement Loci

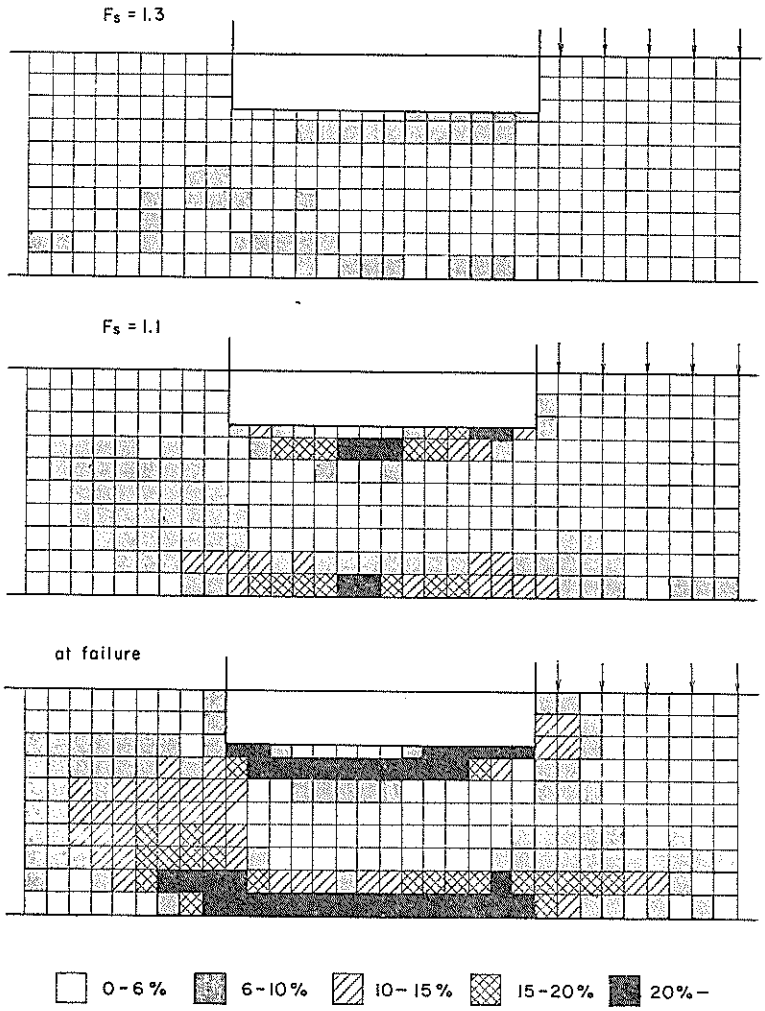

Fig. 16 Shear Strain Distribution

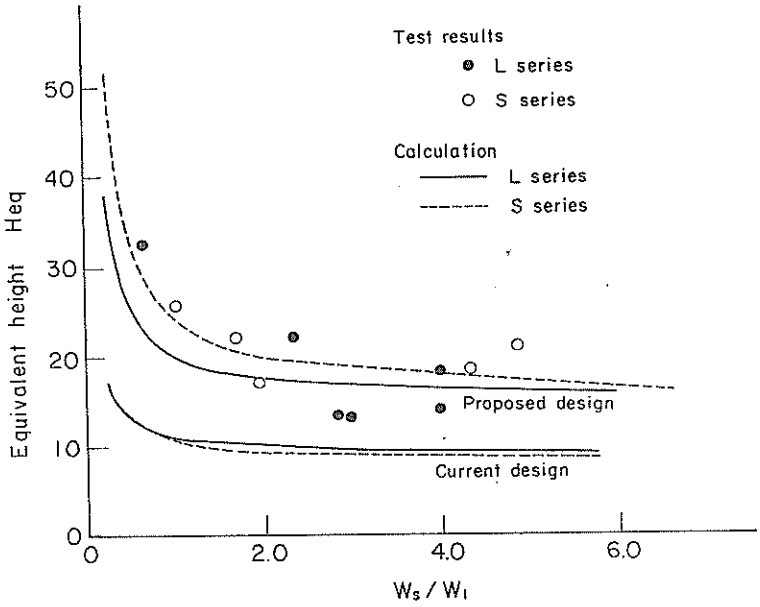

Fig. 17 Equivalent Height, H_{eq}

(2) Boundary Stresses of the Rigid Buried Structure

Both in the calculation of external and internal stability of a rigid buried structure, rigorous determination of the stresses acting on the boundary of the buried structure is important. A series of model tests has been carried out for the buried structure resting on the reliable sandy layer and that floating in the soft clay. Study is still in progress but a part of which has been submitted to 11 th ICSMFE and to 20 th annual JSSMFE

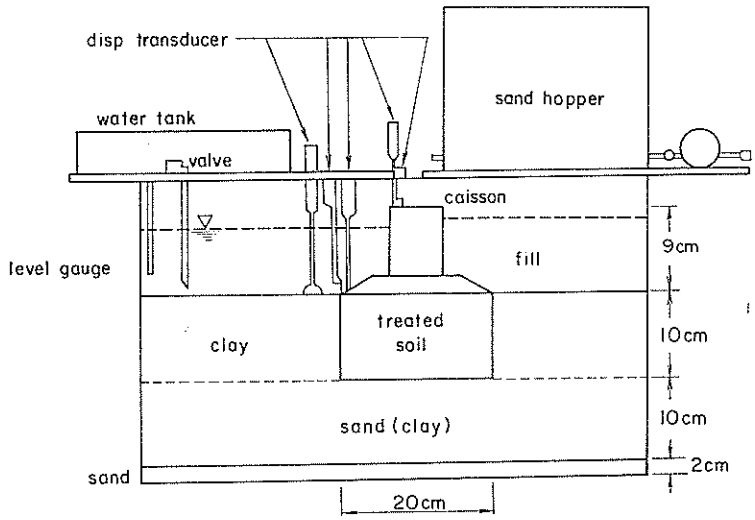

Fig. 18 Setup of Model Ground

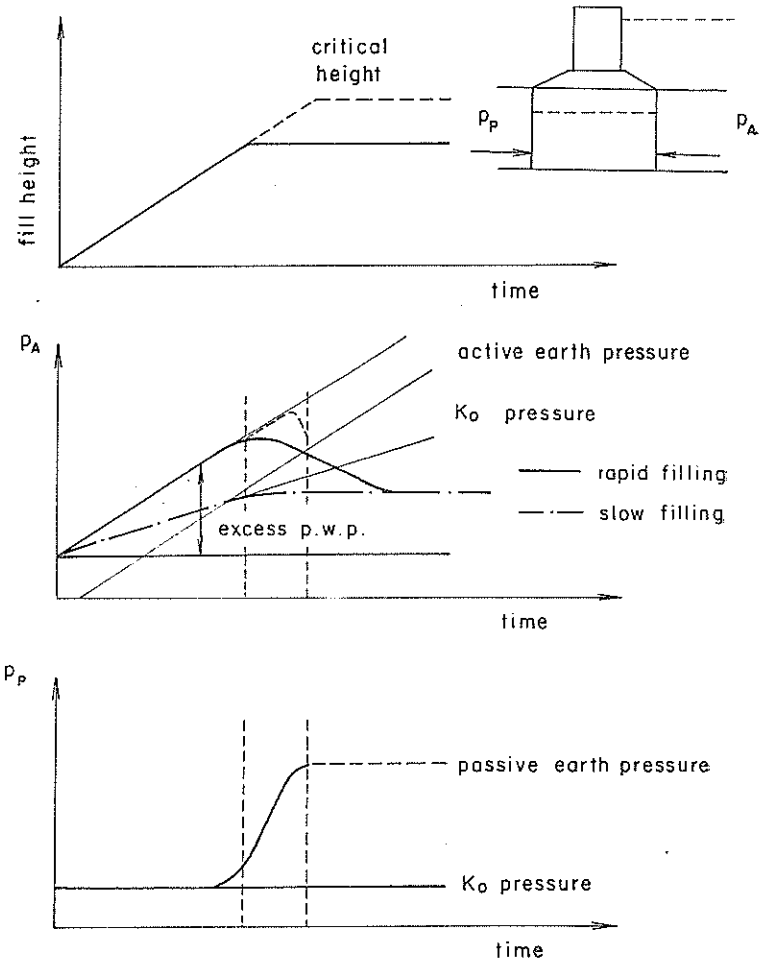

Fig. 19 Concept of Earth Pressure Change

Meeting (Terashi et al. 1985 a, Terashi et al. 1985 b).

These model tests have no specific prototype and the purpose of the study is to know the interaction between soft soil and extraordinary stiff treated soil mass. Soft clay was modeled by Kaolin and the treated soil by bakelite. Rigid structure of treated soil is placed on a sand or on the pre-consolidated clay layer in the prescribed position in the strong box. Kaolin remolded by a vacuum mixer at high water content is poured around the buried structure and pre-consolidated on the laboratory floor under low pressure. Then the strong box was mounted on the swinging platform of the centrifuge, and brought into high acceleration field for self-weight consolidation. After more than 20 hours flight, normally consolidated clay ground improved by DMM is prepared. Centrifuge is once stopped to manufacture gravel mound and to place a concrete caisson on top of the mound. Acceleration is increased once again and backfilling is carried out by sand raining in flight by means of sand hopper. The measurement of the boundary stresses is carried out by means of earth pressure transducers and pore water pressure transducers embedded in the structure. Setup of the model ground is shown in Fig. 18.

In Fig. 19, earth pressure change during backfilling is schematically shown for the case where the rigid structure is resting on sand. When the fill height is increased rapidly to the critical height (to sliding failure), the earth pressures reach to the active and the passive states finally. It is the condition of external instability. However, if the fill height is lower than the critical height which is the case for actual structure, the earth pressure increment is affected by the factor of safety and rate of filling. When the margin of safety is sufficiently large and if the rigid buried structure does not exhibit displacement during filling, then the earth pressure is dependent only on the rate of filling. In the case of rapid filling, the fill pressure is solely carried by the excess pore water pressure. On the other hand, if the rate of filling is sufficiently low as to allow the dissipation of excess pore water pressure, the horizontal pressure acting on the buried structure is an earth pressure at rest under the fill. Real phenomenon will be somewhere between these extremes and the design loads for internal stability analysis must be determined taking this phenomenon into account. Pressure change is also influenced by the stiffness of the soil underneath the buried structure.

Results of a series of model tests were consistent both qualitatively and quantitaively with the above mentioned concept. Among a series of tests, two model test restlts during rapid filling are selected for comparison (Fig. 20). The rigid structure is resting on a stiff sand layer and is very much stable against external stability (Case A), whereas the structure is floating in the soft clay and is on the verge of sliding failure when the prescribed fill is placed rapidly behind the caisson (Case B). In both cases, the pressure increment acting on the structure from fill side increases rapidly with increasing fill height and whose magnitude is equivalent to the fill pressure. Contrary to this similar tendency in the pressure increase at fill side, the pressure increment in the opposite side of the structure is much different in these two cases. Earth pressure did not change in Case A because almost no horizontal displacement occurred during backfilling, whereas in Case B earth pressure approached to the passive state because sufficient displacement was caused by the fill pressure. This difference in the force increment in horizontal direction gives rise to a large difference in the distribution of the bottom reaction also.

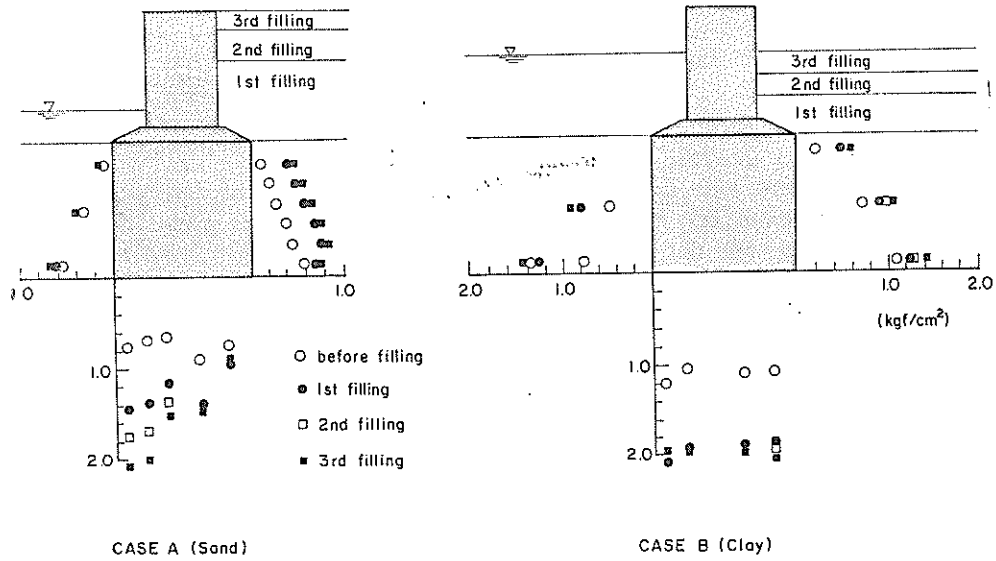

Fig. 20 Boundary Stress Change with Rapid Back Filling

(3) Simulation of Large Scale Experiment

A full scale revetment was constructed on th improved ground and loaded by the backfilling to failure. This large-scale field experiment was carried out as a part of a feasibility study for the new international airport construction in Osaka Bay by the Third District Port Construction Bureau with the cooperation of Port & Harbour Research Institute. The experiment was aimed to investgate the internal stability of treated soil

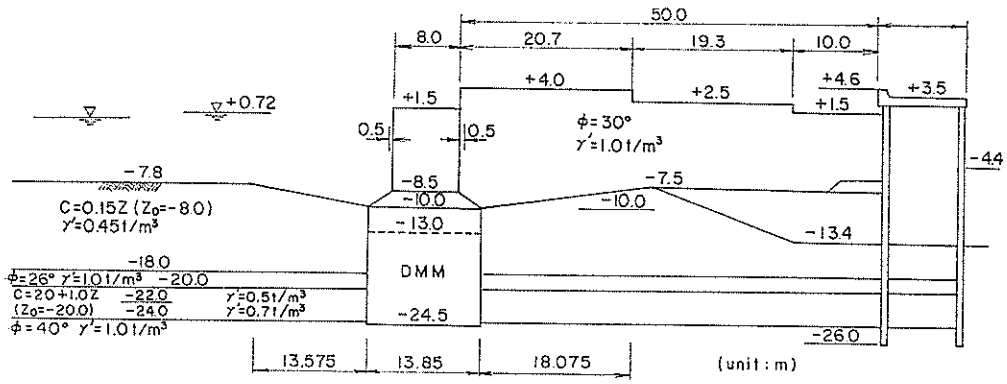

Fig. 21 Sakai Full Scale Experiment

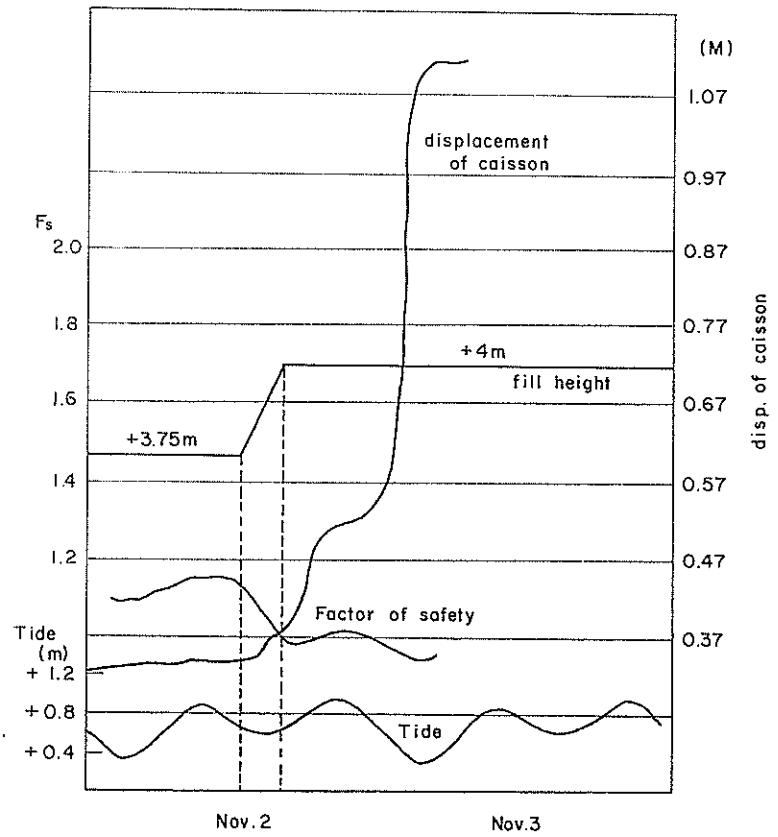

Fig. 22 Displacement of Full Scale Structure

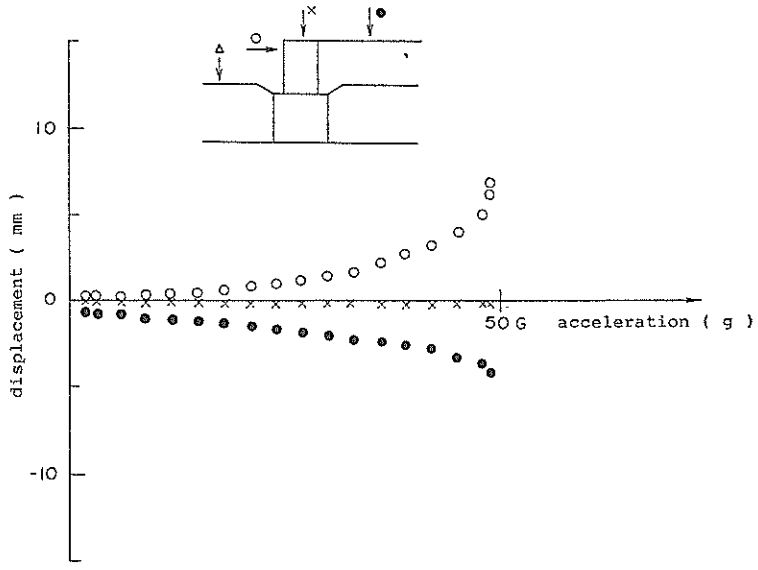

Fig. 23 Displacement of Model Structure with Increasing g

mass of wall type. The superstructure and soil improvement work (Fig. 21) were designed by following the current design procedure. At the final stage of loading by sand fill, the magnitude of induced stress was expected to cause local failure of treated soil mass. But at the same time, the final loading was expected to cause sliding of superstructure which was a concrete caisson in this case. More than 300 sensors were installed in the improved ground, and continuous measurement was carried out throughout the experiment. Details of the test results were given by Yajima and Terashi (1984). In short, the experiment ended with sliding of superstructure, and no evidence of local failure of treated soil mass was observed. Horizontal displacement of the caisson, fill height, tidal change and the calculated factor of safety against sliding of the superstructure were shown in the Fig. 22 for the period of two days approaching to failure.

To supplement the full scale experiment, a centrifuge model test was conducted at the scale of 1/50. The displacement of model caisson with increasing g level is shown in Fig. 23. Failure of the superstructure was at 50 g by sliding. Again in the model, no evidence was found of the failure of treated soil mass. Even though this is a case of simple failure mode, the potential use of centrifuge for modeling site-specific prototype is evaluted.

(4) Bearing Capacity of A Row of Treated Soil Walls

The bearing capacity of a row of treated soil walls (Fig. 12) is a problem of bearing capacity of deep rectangular foundations interfered each other. This problem has also been tackled by centrifuge modeling but with the simple situation of the interference of two closely spaced two dimensional footings on sand under concentric vertical loading at first. And then in the next step, the problem is simplified to the interference of three dimensional footings on sand also under concentric vertical loading (Terashi et al. 1985 c). Figure 24 a) show the change of bearing capacity due to the interference of two footings. The vertical axis of the figure is a bearing capacity of one of the two footings normalized by the bearing capacity of single isolated footing. The horizontal axis shows the spacing and width ratio of the two footings. Figure 24 b) shows the effect of interference

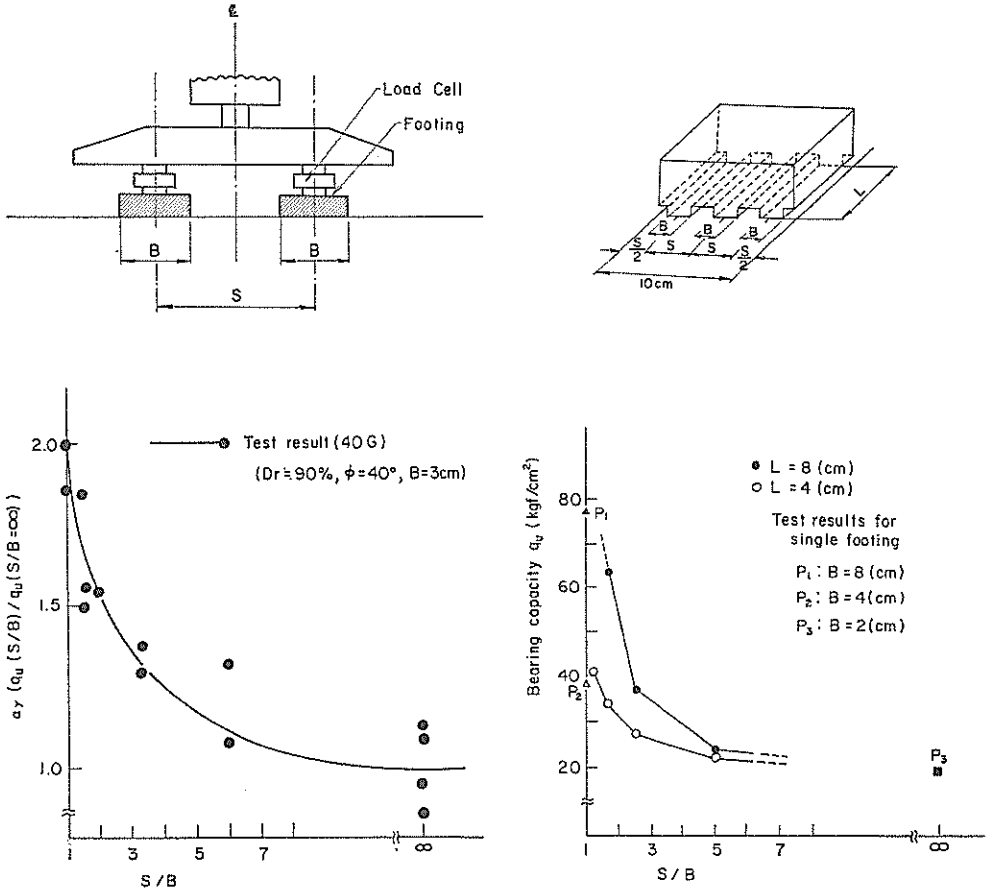

a) Two two dimensional footings b) Three dimensionalfootings

Fig. 24 Interference of Footings on Sand

for three dimensional footings. The vertical axis in the case shows the bearing capacity of one footing.

Further studies are still under way to simulate the actual condtions of deep walls.

4.2 Bearing Capacity of Sandy Ground

The harbor area is almost always protected by breakwaters against incoming waves to keep the calmness of internal water and to maintain the required basin depth. In most cases in Japan, an upright breakwater of composite type is preferred which is usually composed of concrete caisson and rubble mound (Fig. 25). Increase in the volume of domestic and international trades necessitates the renovation and expansion of existing port function and harbor area, which, in turn, results in the necessity of larger breakwaters at deeper sea than ever. Breakwaters also function to reduce the energy of earthquake-originated TSUNAMIs which have often attacked the coast line of northern Japan. For that purpose, also, huge breakwaters are required at deeper sea. These new breakwaters subjected to large horizontal forces and moments raise a new problem to be solved.

The superstructure is designed against the sliding, overturning and bearing capacity at the upper surface of rubble mound. The external forces and bottom reaction acting on

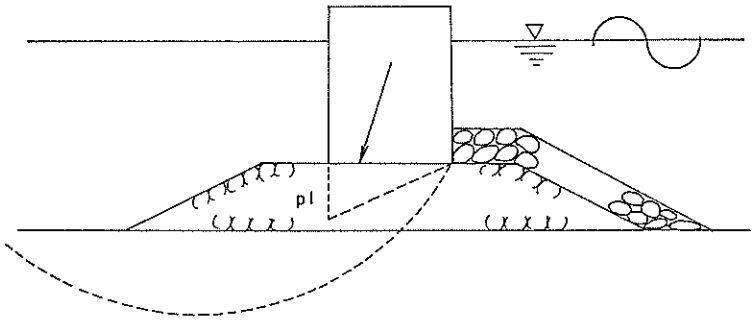

Fig. 25 Composite Breakwater

a superstructure in wave or seismic condition are considered as shown in Fig. 25. Restriction on the bearing capacity posed by the available technical standard in Japan is twofold. The first restriction is essentially a problem of the bearing capacity of two layered soil composed of rubble mound and sandy soil subjected to eccentric and inclined loading. The second restriction is on the toe pressure, p_1 of the superstructure at the surface of rubble mound. By the current design procedure, the magnitude of p_1 is limited to be lower than 50−60 tf/m^2 irrespective of the scale and shape of the superstructure. The available technical standard mentioned above is a product of accumulated experiences of Japanese port construction and rigorous civil engineering considerations. However, neither case history nor theoretical background is given as the reason for the second restriction. It might be the empirical restriction to reduce the excessive tilt and displacement of superstructure by flattening the bottom reaction. In the recent design practice of large-scale breakwaters, however, it is found to be impossible to obtain economical cross section mainly due to the second restriction of the standard. In order to make a large-scale breakwater feasible, urgent study is required to estimate the deformation and ultimate bearing capacity of such a two layered ground under eccentric and inclined loading. This problem was actually the first problem tackled by means of PHRI centrifuge. Therefore, in the course of the study, various techniques and various equipments related to modeling have been studied, developed, and put into practice; the multiple sieve method of sand raining to prepare uniform sand layer of arbitrary chosen density, loading devices, displacement transducers working at high g, and etc.

(1) Bearing Capacity of Concentric and Eccentric Loadings

The bearing capacity of shallow foundation is reduced considerably by load eccentricity. Widely accepted explanation for this phenomenon is based on a concept of effective width $B-2e$ proposed by Meyerhof (1953) where B is the width of actual footing and e eccentricity. A number of research workers have tackled the same problem experimetally and obtained the bearing capacity fairly in good accordance with Meyerhof's hypothesis. At the very beginning of the study of the eccentric inclined loading on a two layered ground, the author has chosen a simple problem of comparing concentric and eccentric vertical loads on a uniform sandy layer.

A series of experiments has been carried out on dense Toyoura sand ($Dr=95\pm5$ %). Results of concentric loading are shown in Fig. 26. In the figure, the abscissa is the generalized width of footing Bn multiplied by the density of sand and the ordinate is the bearing capacity factor. In the experiments the actual footing width B was varied to 0.5, 1, 2, 3, or 4 cm under various accelerations n (g). The generalized footing width is $B\times n$. As shown in Fig. 26 $N\gamma$ for the same Bn value is constant for the actual footing

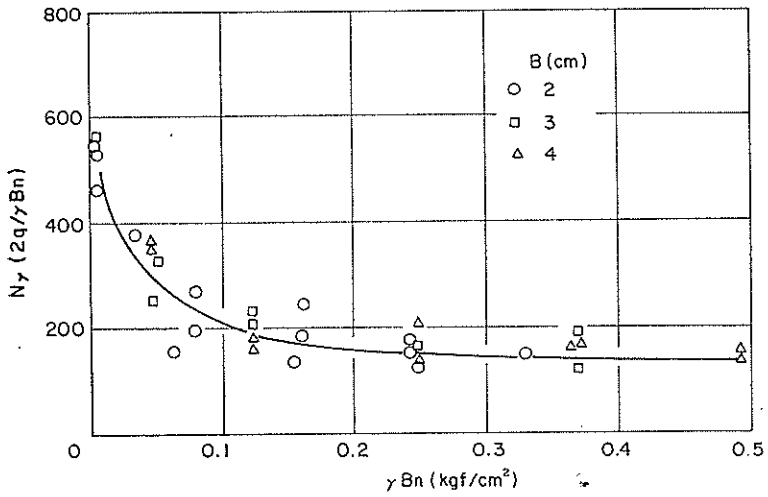

Fig. 26 Bearing Capacity Factor with Varying Bn

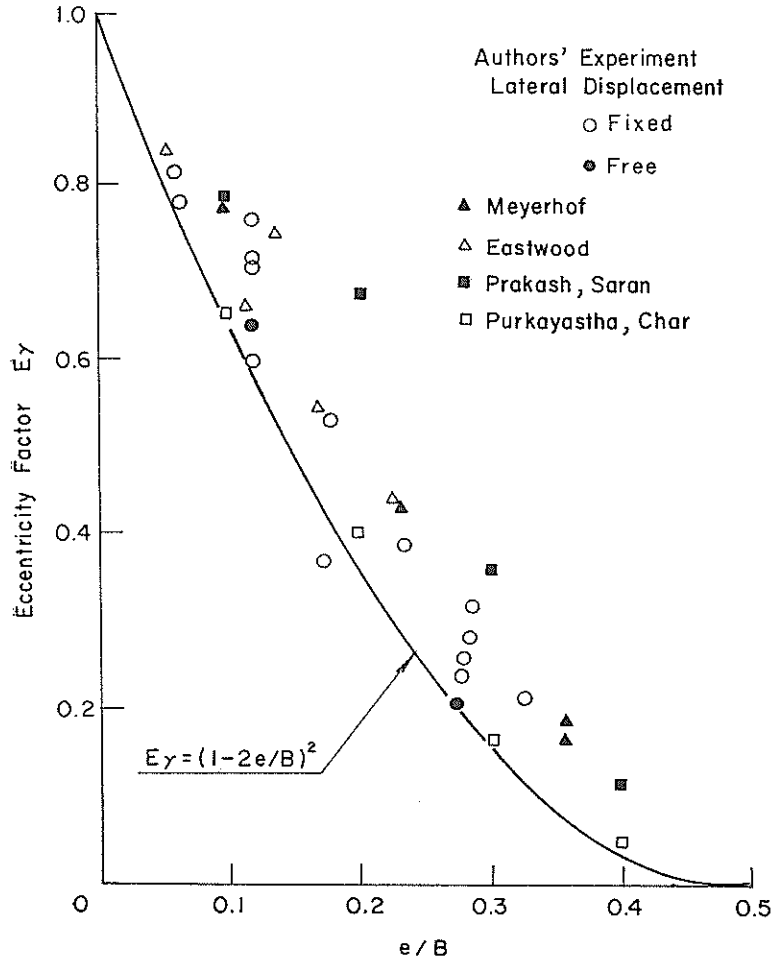

Fig. 27 Reduction of Bearing Capacity by the Load Eccentricity

width B equal to or larger than 2 cm. However, for the footing whose width is less than 2 cm, the bearing capacity was different due to grain size effect. This is a sort of modeling of the model to check the grain size effect. Another finding from this figure is the footing scale effect on the bearing capacity, which was suggested by de Beer (1967) based on the field test data. As Yamaguchi et al. (1976/1977) have pointed out from their centrifuge test results, the scale effect on the bearing capacity is clearly observed irrespective of the actual footing width. The scale effect becomes negligibly small with the increase of γBn if γBn exceeds 0.1.

Thus the test conditions for eccentric loading are determined as $Dr=95\pm 5$ %, $B=4$ cm, and $N=56.25$ g, which result in $\gamma Bn=0.36$. These conditions are decided to avoid both the grain size effect and the scale effect on the eccentric loading test results.

The reduction of bearing capacity with the increase in eccentricity has been obtained from a series of centrifuge tests as shown in Fig. 27. The reduction factor due to eccentricity $E\gamma$ is defined as q_e/q, where q_e and q are the bearing capacities for eccentric and concetric loading respectively. Available test data by different authors and Meyerhof's hypothesis $E\gamma=(1-2e/B)^2$ are also shown in the same figure.

Under the action of eccentric load, the rupture surface becomes one-sided. However there is a contradiction between most of past workers and Jumikis (1956) regarding the direction of the rupture surface. By a series of tests and elasto-plastic FEM, it was concluded that the difference was due to the unexpected development of horizontal force at the loading point which would not give large influence on the bearing value but would change the rupture surface drastically (Kitazume, 1984). The best possible care must be paid in the simplification of the loading condition of prototype and in the design of loading device for model testing.

(2) Bearing Capacity of Two Layered Soil

Failure mode of the two layered soil as in the case of rubble mound underlain by a sand layer may be roughly divided into two patterns. One is the failure mode where no part of the slip surface passes through the underlying soil. The other is the failure mode where a part of the slip surface passes through underlying layer and the bearing capacity is strongly influenced by the strength of the underlying layer. To see the change of failure mode, a series of concentric vertical loading tests on the two layered soil is being carried out as a part of preliminary study. The two layered soil in this case is composed of dense upper layer and medium dense lower layer. Also the concentric vertical loading test has been started for the trapezoidal soil by changing the distance of the footing to the shoulder of the slope. The details of the test results will be reported elsewhere.

4.3 Behavior of Normally Consolidated Clay Ground

(1) Soil Reinforcement by Geotextile

Model tests to reveal the effect of geotextile reinforcement on the soft clay foundation under the embankment load has been just started. Kaolin clay was pre-consolidated on the laboratory floor by the small pressure and brought into the high g field for the self-weight consolidasion. The normally consolidated clay having a thin surface layer of over-consolidated clay is thus completed in the centrifuge. Then the embankment is constructed during flight using sand hopper. Preliminary study included one embankment loading test on untreated ground and two tests on the clay ground reinforced by unwoven fabrics. Test on the untreated ground exhibited a shallow circular slip surface including the toe of the embankment (Fig. 28 a)). Whereas the reinforced ground exhibited no failure under the embankment much higher than that for untreated ground (Fig. 28 b)). Comparison of the shear strain distributions of the untreated and the reinforced ground is suggesting that the potential slip surface of the reinforced ground becomes much deeper

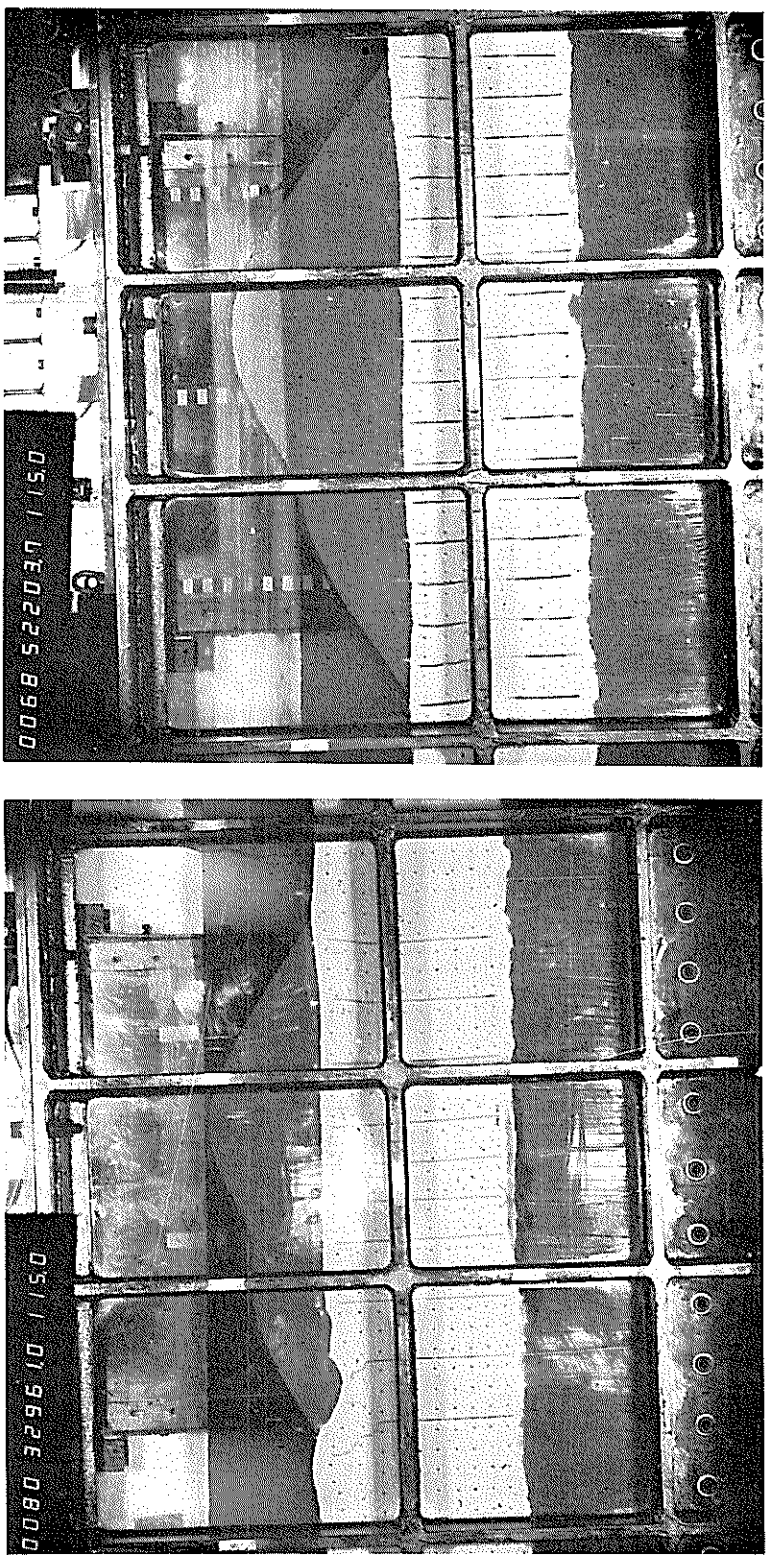

a) Failure of Untreated Ground　　b) Reinforced Ground by Geotextile

Fig. 28 Deformation of Soft Clay under Embankment Load

than that of the untreated soil (Terashi and Kitazume, 1985).

(2) Light Weight Breakwater Directly Seats on the Clay

Usually a breakwater is designed to resist horizontal force by the base friction resulting from the 'own weight of a superstructure. When the foundation ground is soft clay, soil improvement by replacement method and rubble mound construction precede the placement of superstructure.

In the project of new Kumamoto Port where both the wave force and earthquake-induced inertia force are small, a feasibility study of the application of a light weight breakwater is currently carried out by the Fourth District Port Construction Bureau to reduce the initial construction cost. In the case, the basic idea is to reduce the residual settlement and to increase the safety of bearing capacity as well by reducing the weight of the superstructure. However, in the calculation of sliding of such a structure, only the adhesion at the bottom of the structure is the source of resistance to horizontal force if the bottom of the structure is flat. Full scale loading tests of two superstructure of different bottom shape are scheduled toward the end of 1985. To supplement the full-scale tests, a series of centrifuge tests to observe the deformation of the structure during construction phase and a series of tests for bearing capacity of clay under eccentric inclined loading are just started by the request of the Bureau.

4.4 Scope of the Future Studies

Other than the topics described above, modeling of pile or sheet pile structures is also scheduled in a near future. All those static problems have been and will be studied in the Soils Division. The other topic is seismic modeling. Dynamic soils research group in the Structures Division headed by Dr. Tsuchida has just started a preliminary trial for liquefaction study using the PHRI centrifuge.

It is often mentioned by various authors that the modeling by centrifuge can reproduce realistic stresses and hence quite useful in the verification of the theoretical consideration. However, in the case where the simulation of the behavior of a particular prototype is required, one may encounter difficulties in modeling the prototype within a small package and preparing a complicated soil conditions. Fortunately, Port & Harbour Research Institute has close relationship with the Bureau of Ports and Harbours and the District Port Construction Bureaus, Ministry of transport, and is in a good position to obtain detailed data of the prototype behaviors. The soils group at the Institute can carry out full scale tests at site as a part of its research project sometimes. The author believes the comparison of full scale behavior and model test results will bring him important information on the power and limitation of centrifuge modeling of the site-specific prototype.

5. Concluding Remarks

The largest geotechnical centrifuge in Japan was developed at the Port and Harbour Research Institute in 1980. Ancillary equipments were developed in the following two years. Since 1932 various research projects were started using the centrifuge

In the present article the author summarized the importance of the consideration of similarity in model testing and the similarity conditions for the centrifuge modeling. PHRI centrifuge and ancillary equipmsnts were described in detail together with the centrifuge tests results to demonstrate the modeling techniques currently available for the centrifuge.

As described in the previous chapters, PHRI belongs to the Ministry of Transport which is responsible for the design and construction of port and airport facilities. Great

demands exist to simulate not only the ideal prototype-scale structures but also the site-specific prototypes. This challenging but fairly difficult field of centrifuge application will be one of the major subject of the PHRI centrifuge in a near future.

(Received on June 29, 1985)

Acknowledgments

In the course of planning, design, and construction of the PHRI centrifuge, Professor A. N. Schofield of Cambridge University, Professor T. Kimura of Tokyo Institute of Technology, and Professor M. Mikasa of Osaka City University encouraged the author and gave him kind advice and detailed information. Most of those information are reflected somehow to the design of the PHRI centrifuge.

References

1) Avgherinos, P. J. and Schofield, A. N. (1969) Drawdown failure of centrifuged models, *Proc. 7th ICSMFE*, Vol. 2, pp. 497-505.
2) De Beer, E. (1965) Bearing capacity and settlement of shallow foundations on sand, *Proc. Symp. on Bearing Capacity and Settlement of Foundations*, Duke Univ., pp. 15-33.
3) Eastwood, W. (1955) The bearing capacity of eccentrically loaded foundations on sandy soils, *Structural Engineer*, Vol. 23, No. 6, 181-187.
4) Jumikis, A. R. (1956) Rupture surfaces in sand under oblique loads, *Proc. ASCE*, Vol. 82, SM-1, 1-26.
5) Kawasaki, T. et al. (1981) Deep Mixing Method using cement hardening agent, *Proc. 10th ICSMFE*, Vol. 3, 721-724.
6) Kawasaki, T. et al. (1983) Ground stabilized by Deep Mixing Method, *Proc. 7th Asian Regional Conf. on SMFE*, Vol. 1, 249-254.
7) Kitazume, M. (1984) Influence of loading condition on bearing capacity and deformation, *Proc. International Symp. on Geotechnical Centrifuge Model Testing*, 149-151, Tokyo.
8) Meyerhof, G. G. (1953) The bearing capacity of foundations under eccentric and inclined loads, *Proc. 3rd ICSMFE*, Vol. 1, 440-445.
9) Mikasa, M. et al. (1969) Centrifugal model test of rockfill dam, *Proc. 7th ICSMFE*, Vol. 2, pp. 325-339.
10) Okumura, T. and Terashi, M. (1975) Deep Lime Mixing Method of stabilization for marine clays, *Proc. 5th Asian Regional Conf. on SMFE*, Vol. 1, 69-75.
11) Ovesen, N. K. (1985) The application of the Theory of modelling to centrifuge studies, Draft state of the art-Geotechnical centrifuge modeling, *11th ICSMFE*, (will be published by Balkema).
12) Prakash, S. and Saran, S. (1971) Bearing capacity of eccentrically loaded footings, *Proc. ASCE*, Vol. 97, SM-1, 95-117
13) Purkayastha, R. D. and Char, A. N. (1977) Stability analysis for eccentrically loaded footingss, *Proc. ASCE*, Vol. 103, GT-6, 647-651.
14) Rocha, M. (1957) The possibility of soil mechanics problems by the use of models, *Proc. 4th ICSMFE*, Vol 1, pp. 183-188.
15) Roscoe, K. H. (1967) Soils and model tests, *J. of Strain Analysis*, Voo. 3, No. 1, pp. 57-64.
16) Terashi, M., Tanaka, H. and Okumura, T. (1979) Engineering properties of lime-treated marine soils and DM method, *Proc. 6th Asian Regional Conf. on*

SMFE, Vol. 1, 191-194.

17) Terashi, M. and Tanaka, H. (1981) Ground improved by Deep Mixing Method, *Proc. 10 th ICSMFE*, Vol. 3, 777-780.

18) Terashi, M. and Tanaka, H. (1983) Settlement analysis for Deep Mixing Method, *Proc. 8 th ECSMFE*, Vol. 2, 955-960.

19) Terashi, M. et al. (1983 a) Development of qualitative photoinstrumentation system by means of 70 mm data camera & analyzer, *Optical Systems Engineering III*, William H. Taylor, Editor, *Proc. SPIE 389*, 62-74.

20) Terashi, M., Tanaka, H. and Kitazume, M. (1983 b) Extrusion failure of ground improved by the Deep Mixing Method, *Proc. 7 th Asian Regional Conf on SMFE*, Vol. 1, 313-318.

21) Terashi, M. and Kitazume, M. (1985) Centrifuge study on the reinforcement of soft clay by geotextiles, *Interim report prepared for the Coastal Development Institute of Technology* (in Japanese)

22) Terashi, M., Kitazume, M. and Yajima, M. (1985 a) Interaction of soil and buried rigid structure, submitted to *11 th ICSMFE*.

23) Terashi, M., Kitazume, M. and Akamoto, H. (1985 b) Interaction of soft clay and deep foundation, *Proc. 20 th Annual Meeting of JSSMFE*, pp. 1635-1638 (in Japanese)

24) Terashi, M. et al. (1985 c) Interference of shallow footings on dense sand, *Proc. 20 th Annual Meetlng of JSSMFE*, pp. 1023-1026 (in Japanese)

25) Yajima, M. and Terashi, M. (1984) Full scale loading test on the improved ground by DMM. *Proc. JSSMFE Symp. on the Strength and Deformation of the Composite Ground*, pp. 67-74 (in Japanese).

26) Yakovleva, G. (1985) Use of geotechnical centrifuge in the USSR, Draft state of the art-Geotechnical centrifuge modelling, *11 th ICSMFE*, (will be published by Balkema).

27) Yamaguchi, H., Kimura, T. and Fujii, N. (1976) On the influence of progressive failure on the bearing capacity of shallow foundations in dense sand, *Soils and Foundations*, Vol 16, No. 4, 11-22.

28) Yamaguchi, H., Kimura, T. and Fujii, N. (1977) On the scale effect of footings in dense sand, *Proc. 9 th ICSMFE*, Vol. 1, 795-798.

Appendix A: Photographic Instrumentation System

A. 1. Object and Its Condition for Photo-instrumentation

(1) Outline of object

The object to be photographed (model ground) and requirements for instrumentation are outlined in the following. For the large specimen container shown in Fig. A. 1, the size of the transparent window is 400 mm×700 mm and is made of acrylic resin of 120mm thick. Photographs of the model ground in the specimen container can be taken from two positions of the pit; the one is the opening at the side wall of the concrete pit, the shoot-

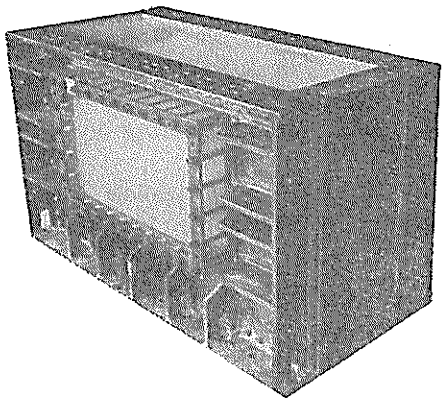

Fig. A. 1 Specimen Box with a Transparent Side

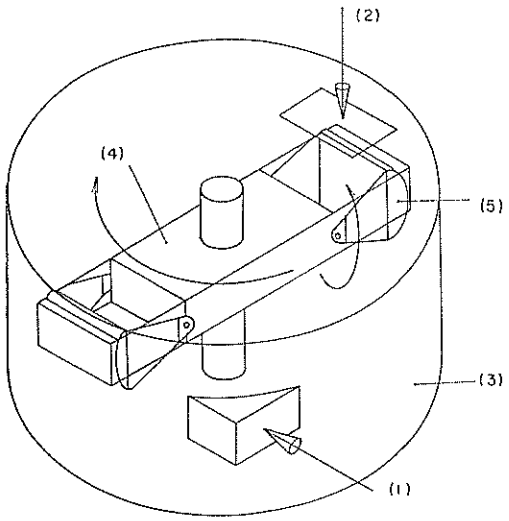

Fig. A. 2 Schematic View of Centrifuge

This appendix is a summary of the paper by Terashi et al[1]

ing window I and the other is the opening at the upper floor of the pit, the shooting window II as shown in Fig. A. 2. The shooting windows are also made of acrylic resin of 50 mm thick. The distance between the camera and the object is 4500 mm for the former and 2500 mm for the latter shooting window.

(2) Velocity of the object

The velocity of the object is calculated as follows;

$$v = r\ \omega \qquad (1)$$

where, v : speed of the object (m/s)
r : radius of the object (3.6−3.8 m)
ω : angular velocity of centrifuge (radian/s)

Therefore, at the maximum rotation of 165 rpm the velocity of the object is 62−66 m/s.

(3) Sampling rate

In order to follow the changing behavior of the model ground, it is desirable to take a sufficient number of photographs. The maximum sampling rate is hence set to cover the maximum rotation of centrifuge, 165 rpm. The camera is planned to be fixed to the concrete pit as described above.

(4) Auxiliary data recording

A number of still photographs are taken for a particular model test and should be analyzed with other data obtained by electrical measuring devices. Therefore, an auxiliary data superimposing device is required to correlate photographic data with other data. The time (s), rotational frequency (rpm), and consecutive frame number are selected data to be superimposed on the photographic image.

A. 2. System Study for Data Acquisition

A. 2.1 System Outline

What the centrifugal modeling requires is a non-contact measuring device of the displacement on the model ground during flight. There are two alternatives of optical techniques to acquire data under the prescribed conditions, e. g., film or TV.

The TV system has the advantages of real time observation and quick playback with the aid of video tape recording. But it also has the following disadvantages; poor resolving power, limited amount of image information and large image distortion when compared with the still photography. If it is assumed that the TV system is introduced in the present test condition, the object (400 mm×700 mm) must be measured by 525 scanning lines of conventional TV. It means the minimum unit of accuracy is 0.76 mm on the image and the accuracy may be further reduced due to various factors distorting the image. Therefore, the film system is superior in the case of precise measurement of deformation and the TV system is superior in the real time observation.

There are also many alternatives in film system. The type of film is the major factor determining the accuracy and amount of data in the film system. The type of film is described by film size, film sensitivity, film base and resolving power. To record the model behavior changing with the lapse of time, a roll film is most convenient. The film size governs the data quality in the sense that a larger format film can record a large amount of information in it. The amount of information of 70 mm film format (57 mm× 57 mm) is 42 times as large as that of 16 mm film format (10.3 mm×7.5 mm).

There are also many variations in the method of digitizing film image, e. g., precise measurement using microscope, combination of projector and digitizer or automatic photo-digitizer system using computer. Accuracy, efficiency and cost must be considered for

particular purposes of the system.

Based on the consideration on each component described later, the system diagram as shown in Fig. A. 3 was concluded suitable for the analysis of PHRI centrifuge. The system consists of;

i) system controller
ii) pulse data camera
iii) light source
iv) projector
v) digitizer
vi) data processor

As the object is flying by high speed, a short duration light source is necessary to fix the object as a stationary image on the film. It is also necessary to detect the position of the object to take photographs at constant positions. The system controller should, therefore, detect the position of flying object and control the camera and light source by electrical signals. The controller also has to generate numerical data to be superimposed on the film. On these conditions, a combination of data camera and flash unit driven by pulse signal is considered. The film image thus taken is read by a digitizer. The coordinates obtained by the digitizer contain various errors that arise in the process of transforming the object to the coordinates by the system. A data compensating process is introduced to the system by the aid of microcomputer.

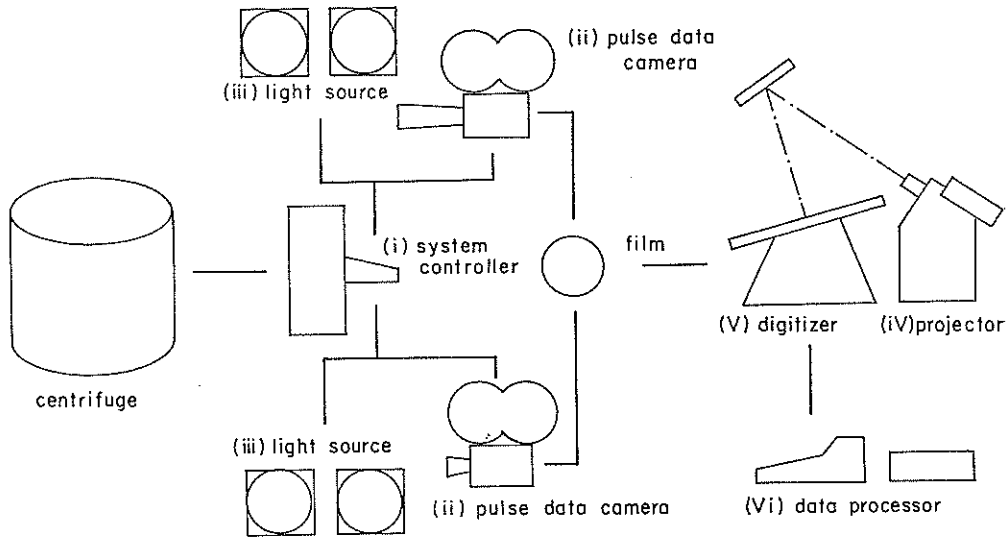

Fig. A. 3 System Diagram of Photo-instrumentation

A. 2. 2 Requirements for Each Component

The ideal photography reproduces the object with complete fidelity, but actual photography cannot do so because of various errors and limitations. In the following paragraphs various factors causing errors and limitations are discussed for each component of the photo-instrumentation system.

(1) Film

Film is the medium for recording the image focused on it by lens. The characteris-

tics of the film that affect the quality of the measurement are ;

a) resolving power
b) photo-sensitivity
c) dimensional stability
d) film size

From the view point of quantity of measurement, film capacity should be considered in addition to the above mentioned factors. Resolving power is the ability of the film to record distinct images of small or contiguous objects. In general there is a relation

Table A. 1 Characteristics of Black and White Instrumentation Films[2)]

Films	Color Sensitivity	photo Sensitivity	Resolving Power (for T. O. C. =1000 : 1)	Applications & Special Properties
RAR 2495 (ESTAR-AH-Base)	Ortho	320	100	CRT recording
RAR 2479 (ESTAR-AH-Base)	Extended Red Pan	500	100	For outdoor and artificial light
LINAGRAPH SHELLBURST 2476 (ESTAR-AH-Base)	Extended Red Pan	200	160	For cinetheodolite photography of aerial objects
Pan 2484 (ESTAR-AH-Base)	Pan	800	63	For weak illumination

Table A. 2 Dimensional Change Characteristics of Films[3)]

Characteristics	Film Base			
	Triacetate Base		ESTAR Base*	
base thickness (mil)	5. 25		4	
typical emulsion type	B & W		B & W	COLOR
gel/base ratio	0. 09		0. 08	0. 21
DIRECTION OF TEST	LENGTH	WIDTH	—	—
humidity coefficient of linear expansion (unprocessed) % per 1 % RH	. 0055	. 0065	. 0018	0030
thermal coefficient of linear expansion % per °C	. 005	. 006	. 002	. 002
processing dimensional change range				
% shrinkage	−. 10		−. 03	−. 04
% swell	+. 04		+. 03	+. 03
processing and aging shrinkage (in size)				
1 wk @50°C-20% RH	. 15	. 20	. 03	. 06
1 yr @25°C-60% RH	. 30	. 35	. 03	. 03

*ESTAR is Kodak's trade mark and made of polyester base.

between resolving power and photo-sensitivity; the higher the photo-sensitivity is, the poorer the resolving power is. Resolving power and photo-sensitivity of roll films are shown in Table A. 1[2]. Photo-sensitivity must be high enough to obtain a stationary image of the flying object.

A film changes its size with the change of temperature and humidity and also in the course of processing. A film basically consists of the base from 0.1 mm (4 mil) to 0.13 mm (5 mil) thick and the emulsion layer from 0.01 mm to 0.03 mm thick coated on the base. For the roll film, two types of material are used as the base; triacetate and polyester. Table A. 2 shows that the dimensional stability of polyester is much higher than triacetate[3].

(2) Lens

Lens is one of the most important factor in taking sharp photographs. Especially in the case of photo-instrumentation, performance of the lens must be considered strictly as follows;

a) low distortion ·····high fidelity
b) high resolving power·····precise measurement
c) fast lens·····illumination
d) large format camera lens·····to cope with large format film

Lens has five types of aberrations and there is no lens without these ones. An adequate lens should be chosen in accordance with its purpose of application. General classification of lenses are shown in Table A. 3[4]. Normal lenses (Type A) are not adequate for precise measurement because the distortion in the range from -2% to 1.5% is considered to be negligible for these lenses[5]. The data of the lens considered for the system are listed in Table A. 4[6]. In the table, Apo-El Nikkor is chosen for the camera at the shooting window I. For the camera at the shooting window II, Micro Nikkor was considered at first, but the distortion and aperture ratio are not satisfactory for the present instrumentation system. A new lens was designed for the window II of the present system (NAC lens).

Combined resolving power of the lens and film is estimated by Katz's equation[7] as follows;

$$1/R(fl)=1/R(f)+1/R(l) \qquad (2)$$

where $R(fl)$, $R(f)$, and $R(l)$ denote the resolving powers of lens and film, of film alone, and of lens alone, respectively. From Table A. 1 and A. 4, the combined resolving

Table A. 3 Classifications of Lenses[4]

Lens Type	Applications (Magnification)	Compensated aberration	Compensating condition
Type A	General photographing (inf. – 1 m)	Mainly Spherical aberration. Standard and wide angle	Diffused light INF.
Type B	Micro (Macro) copy (1/20—1/5)	Spherical aberration and Astigmatism	Condensed and diffused light ×10 magnification
Type C	Enlargement (x10—x1)	Spherical aberration and Astigmatism	Condensed light x3 magnification
Type D	Plate making (x2—x1/2)	Distortion and Axial chromatic aberration	Diffused light x1 magnification
Type E	Microscope (x10—x1500)	Spherical aberration	Pure condensed light Fixed magnification

Table A. 4 High-performance Lenses

	Window I : Apo-EL Nikkor f=300mm[6]	Window II : NAC lens f=150 mm	Micro Nikkor f=150mm[6]
Aperture ratio F.	5. 6	4. 0	5. 6
Standard magnification	x 10	x 1/13	x 1/10
Usable magnification	x 5 - 20	—	about x 1/30-1/5
Compensation of chromatic aberration (nm)	380 - 700	400 - 700	400 - 650
Distortion	0 02%	0. 02%	0. 1%
Resolving power (lines/mm)	80	100	150

power of Kodak Linagraph Shellburst 2476 and Apo-El Nikkor f=300 mm gives rise to 53. 3 pair lines/mm. When shootiag magnification is set as $M(s)$, minimum unit to be measured by the combination is theoretically $1/(M(s)\times 2\times 53.3)$ mm.

(3) Camera body

The camera body is not only a black box but must function as follows;

a) to feed the film in response to pulse signal,
b) to press the film on the focal plane flatly,
c) to position the film and lens to prescribed position perfectly, and
d) to superimpose the auxiliary data on the film

The resolving power of lens is reduced by the out-of-focusing. The relation between the resolving power of lens and the gap from focusing plane is expressed by the following equation[8].

$$x=F/\alpha R \qquad (3)$$

where, x : gap from focal plane
R : resolving power of lens
F : iris ratio of lens
α : coefficient of iris shape
α=1 for rectangular iris
α=0. 8 for round iris

When F=5. 6, α=0. 8 and R=80 of the lens for the window I are substituted into eq. (3), x is 0. 088, which means that resolving power of the lens would be secured if the focusing were adjusted by the camera within 0. 088 mm. No adequate camera is available for the purpose of the present system. A new pulse data camera with 70 mm film format has thus been designed.

(4) Light source

Because the object is flying fast, there is no way to give exposure without using a flash unit in order to avoid image blur. The relation between the exposure time and the displacement of the flying object is;

$$D=v\ t \qquad (4)$$

where D is the displacement of the object, v is the velocity of the object, and t is the exposure time (flash duration). Even if the exposure time of 10 microseconds is given, the displacement of the present object is around 0. 7 mm at its maximum rotation. This displacement of the object during the exposure time causes image blur and results in the error in measurement. The magnitudes of the image blur on the photographs taken at different sites (shooting window I and II) are different even if the object is flying by the

same speed. When a photograph is taken from above (at the window II), the object moves perpendicular to the optical axis and every point in the object draws an arc whose lenght is calculated by eq. (4). In the case where a photograph is taken from the tangential direction (at the window I), the object moves along the optical axis with only a sligt displacement visible in the radial direction. On the other hand, the inclination of the object to the optical axis can be maintained constant in the case of photographs taken from the window II, but it inevitably changes in the case of photographs taken from the window I. The effect of the inclination of the object to optical axis is discussed later in detail.

At the window I, if the admissible inclination of the object is taken as 2′ (±1′), the flash duration can be 30 microseconds. The radial displacement of the object during this exposure time is of the order of only 10^{-4} mm. At the window II, the flash duration of only 6 microseconds results in the displacement of the object of 0.4 mm. However, the light intensity of flash is determined by discharging electricity from capacitor and the time history of light intensity takes a shape of sharp rise and slow decay. By this effect, the photographic image of a particular point to be measured is expected to have a core and blur, or that is to say, an image of comet tail. This image may be measured more precisely than the anticipated image which is a dim arc of 0.4 mm long. However, it is difficult to define the error for the image of comet tail quantitatively.

(5) Film projector and digitizer

There are almost the same factors affecting the errors in projection as in taking the photographs. In projection, following additional factors should be considered.

A large amount of heat radiates from the projection lamp and generates a heat problem. Film expansion during digitizing must be avoided as long as possible. A cold reflector, a cold mirror, a cold filter, and a cooling fan are introduced in the projector and designed to restrain the temperature increase of the film within 5 degrees in Celsius. Under this condition, the thermal expansion of ESTAR film is limited within 0.01 %.

The performance demanded for a projection lens is different from that fot a shooting lens. The lens type C in Table 3 is suitable for projection. The lens with large aperture ratio is not nacessary but the distortion should be strictly controlled. EL-Nikkor f=135 mm is selected for the projection lens whose specifications are:

EL Nikkor f=135 mm

aperture ratio	: F 5.6
compensation of chromatic aberration	: 380−700 (nm)
distortion	: +0.025 %
resolving power	: 80 pair lines/mm

In the centrifugal model test, hundreds of small targets are placed on the surface of model ground at the transparent side of the specimen container. Then the deformation of the model ground is measured on a series of photographs as the displacements of these targets from their initial positions. Therefore, photographic images of targets must be digitized with high accuracy and at the same time with high fidelity. Initial arrangement of the targets may be strongly disturbed and some of the targets may become invisible with the lapse of time, because the model ground is usually brought to large deformation or to failure. This makes it difficult to search and digitize the position of each target automatically. Instead, manual digitizing with proper judgement of the operator is chosen in the present system. The minimum measuring unit of human's eye is said to be 0.073 mm when the observation is done at the distance of distinct vision under the condition that the minimum human's look angle is 1′[9]. It is no use applying digitizer with higher resolving power than human's eye. Considering the combination of magnification and the resolving power of digitizer, the Seiko D-Scan was chosen as suitable

digitizer for the present system, whose major specifications are;

a) digitizing method : method of absolute coordinating by electro-magnetic induction
b) digitizing area : 1,000 mm×1,300 mm
c) resolving power : 0.04 mm
d) total accuracy : within ± 0.15 mm
e) output : 16 bit binary

By the present system using 70 mm film and the digitizer, the total magnification of the object to the projected image is calculated as follows;

$$M(t)=M(s)\times M(p) \tag{5}$$

Where $M(t)$, $M(s)$ and $M(p)$ are the total, shooting and projecting magnifications respectively.

$M(s)$=film image size/object size=57/740

$M(p)$=screen size/film image size=1300/57

Thus the total magnification of the present system becomes 1.54.

(6) Orthogonality to the optical axis

Other than the measuring capability of each component, there still remains a factor governing the accuracy of measurement, which is the orthogonality of film, object and projected image to the optical axis. Orthogonality of the film to the optical axis in the camera or in the projector is a problem of manufacturing. While, orthogonality of object or digitizing screen (projected image) is a problem of the accuracy in positioning the camera or projector and also a problem of detection of the position of the flying object.

Inclination of film plate to optical axis is genarally required to be less than 10′ for ordinary 35 mm still camera but limited to be less than 1′ for precise instrumentation. Inclination of the object or projected image must be considered for the purpose of particular system. Measuring error caused by inclination is estimated by the following equation.

$$a'/a=1/(\cos\theta-\sin\theta\times\tan\omega) \tag{6}$$

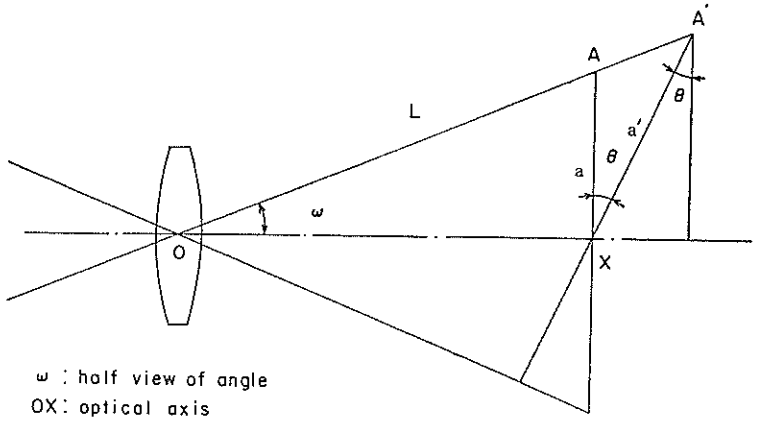

ω : half view of angle
OX : optical axis
θ : inclination of object, film, or screen
$\overline{XA}$: a
$\overline{XA'}$: a′
$\overline{OA}$: L

Fig. A. 4 Geometrical Model for Inclination

Variables in the equation are shown in the geometrical model (Fig. A. 4). XA is the proper position orthogonal to the optical axis and XA′ is the position inclined by the angle θ. When the position of an object is considered, length a' is the actual length on the object but length a is a measured one with error due to inclination. When the projection is in concern, a is accurate one and a' is the measured one. Table A. 5 shows the magnitude of error due to anticipated inclination.

Table A. 5 Error Ratio of Each Positioning

	Object	Camera		Projector	Screen
f (mm)	300	300	150	135	135
ω (°)	5. 04	5. 04	10. 0	11. 4	11. 4
θ (′)	3	1	1	1	3
$\left(1-\frac{a}{a'}\right)\times 100$	0. 0077	0. 0026	0. 0051	0. 0059	0. 017

(7) Estimation of total accuracy of the system without data compensation

As discussed above, the resolution of each component is selected to satisfy the condition of precise measurement of a single target. Total accuracy of the length between different points are considered for various factors affecting the image distortion as tabulated in Table A. 6. As is described earlier, the image blur of the photographs taken from the window II is not estimated quantitatively, and the total accuracy there is left blank. Total accuracy for the window I is estimated by the product of each factors and hence it gives the maximum anticipated error of the system for the window I.

(8) Data compensation

The anticipated maximum error for the measurement of length by the system is ±

Table A. 6 Estimated Total Accuracy of the System Without Data Compensation

	Window I	Window II
Error Factors of photographing		
distortion of shooting lens	0. 02%	0. 02%
thermal expansion of film	0. 01%	0. 01%
humidity expansion of film	0. 01%	0. 01%
processing dimensional change of film	0. 03%	0. 03%
positioning of film	0. 003%	0. 005%
positioning of object	0. 008%	—
Error factors of projecting		
distortion of projection lens	0. 025%	0. 025%
thermal expansion of film	0. 01%	0. 01%
humidity expansion of film	0. 018%	0. 018%
aging shrinkage of film	0. 03%	0. 03%
positioning of film	0. 006%	0. 006%
positioning of digitizer	0. 017%	0. 017%
accuracy of digitizer	0. 015%	0. 015%
Total Accuracy	0. 20%	—

1.69 mm for the diagonal length on the object (0.2 % of 806 mm). This magnitude of error is too large for the analysis of centrifugal model test. Consequently, data compensation process with the aid of fiducial points are necessary to correct the deformed image. Fiducial points must be those points whose exact coordinates are known and which do not deform during the test. When fiducial points are placed to cover all the area to be photographed, various types of distortion, linear and nonlinear, which result in the error of measured coordinates may be compensated. Compensation functions of at most the third order are programmed to correct the measured coordinates of the targets;

$$X=a_0+a_1X+a_2Y+a_3XY+a_4X^2+a_5Y^2+a_6X^2Y+a_7XY^2+a_8X^3+a_9Y^3$$
$$Y=b_0+b_1X+b_2Y+b_3XY+b_4X^2+b_5Y^2+b_6X^2Y+b_7XY^2+b_8X^3+b_9Y^3 \qquad (7)$$

In order to determine the coefficient of cubic equation, a_0 to a_9 and b_0 to b_9, 10 fiduciai points of the known coordinates are necessary. To increase the accuracy of compensation, it is better to place more than 10 fiducials and to determine the coefficient by the least square method.

$$S_X=\sum\{X_\kappa-(a_0+a_1X_\kappa+\cdots\cdots\cdots\cdots+a_9Y_\kappa^3)\}=\min.$$
$$S_Y=\sum\{Y_\kappa-(b_0+b_1X_\kappa+\cdots\cdots\cdots\cdots+b_9Y_\kappa^3)\}=\min. \qquad (8)$$

where κ is the number of fiducial points. Coefficients which satisfy eq. (8) are obtained by solving the following equations;

$$\partial S_X/\partial a_i=0\,,\quad \partial S_Y/\partial b_i=0 \qquad (9)$$

where i is 0 to 9.

A. 3. Specification of the Photo-instrumentation System for PHRI Centrifuge

Based on the requirements on the accuracy of the measurement, the system is designed and each component is specially manufactured or purchased. Major specifications of the system are described in the following paragraphs.

A. 3. 1 System Controller

The controller mainly has four functions; a) detection of the position of flying object, b) sequence control of the camera and flash unit, c) drive control of the pulse data camera, d) superimposing of the auxiliary data. The system controller is shown in the right hand side of Fig. A. 5.

a) Detector of the position of object;
As the object must be taken photographs at the prescribed position where the object becomes orthogonal to the optical axis of the camera fixed to the concrete pit. The magnetic sensor is put on the main shaft of centrifuge.

b) Sequential control;
Basically the pulse signal obtained by the detector is utilized to trigger the camera and flash unit.

c) Drive control of the data camera;
Camera selection modes are provided for the modes of camera I, camera II and camera I & II, and photographing interval modes are available for manual photographing and

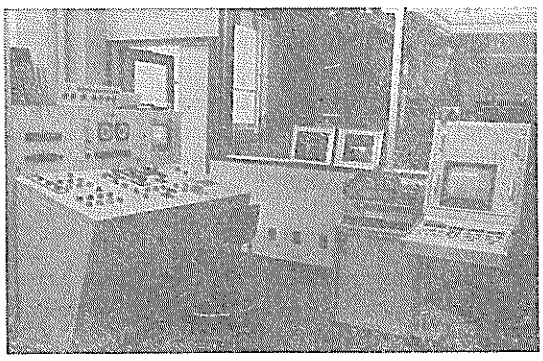

Fig. A. 5 System Controller

automatic photographing of 1 frame per round to 1 frame per 100 rounds.

d) Superimposing of the auxiliary data;

The elapsed time since the beginning of test (s), rotational frequency of the centrifuge (rpm), and consecutive number of the photographs are displayed on the control board for each camera and are superimposed on the photographs. These auxiliary data are also transmitted to the computer if necessary.

A. 3. 2 Pulse Data Camera

The specifications of the pulse data camera (Fig. A. 6) designed for the system is;

a)	drive mechanism	: pulse drive
b)	film speed	: 3 frames/sec maximun
c)	film and its capacity	: 70 mm film Type I 1000 ft (1200 ft with ESTAR)
d)	aperture size	: 57 mm×57 mm
e)	shooting lens	: f=300 mm, F 5.6 for the window I f=150 mm, F 4.0 for the window II
f)	data box	: frame number, 4 digits LED time, 6 digits LED rpm, 4 digits LED
g)	film flathness	: less than 0.02 mm over whole plate is maintained with the aid of vacuum absorption
h)	film orthogonality to the optical axis	: within 1′

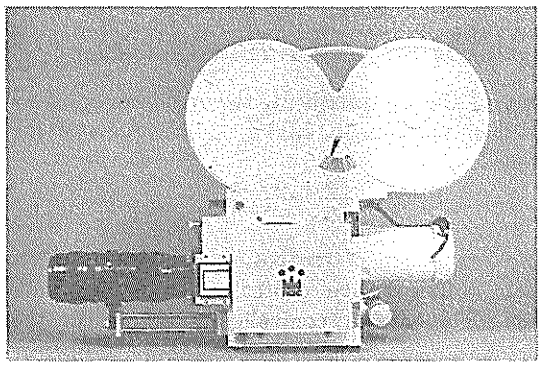

Fig. A. 6 70 mm Pulse Data Camera

The drive mechanism of the camera for the film movement consists of a main motor, reduction gears and a clutch & break assembly. The film feeding mechanism consists of a magazine, sprockets, a tension roller, a vacuum pump and a vacuum plate which feed the film for one frame per one trigger signal from the system controller. Three sprockets, supply, take-up and pull-down are used and a maltese cross mechanism is selected for pulldown sprocket to advance the film. For the auxiliary data, LED number display units, a circuit board, and superimposing optics are equipped to the camera. The superimposing optics consists of a mirror, shooting lens and two prisms. As the exposure time is essentially controlled by the flash duration, the mechanical shutter is supplied just for protecting the film from the unexpected exposure.

A. 3. 3 Light Source

The specifications of the light source are;

		flash unit for window I	flash unit for window II
a)	quantity of flash bulb	2	2
b)	Guide Number (ASA 100)	42	18
c)	flash duration (microsec)	30	6
d)	trigger delay (microsec)	9	9
e)	flash frequency (Hz)	3	3

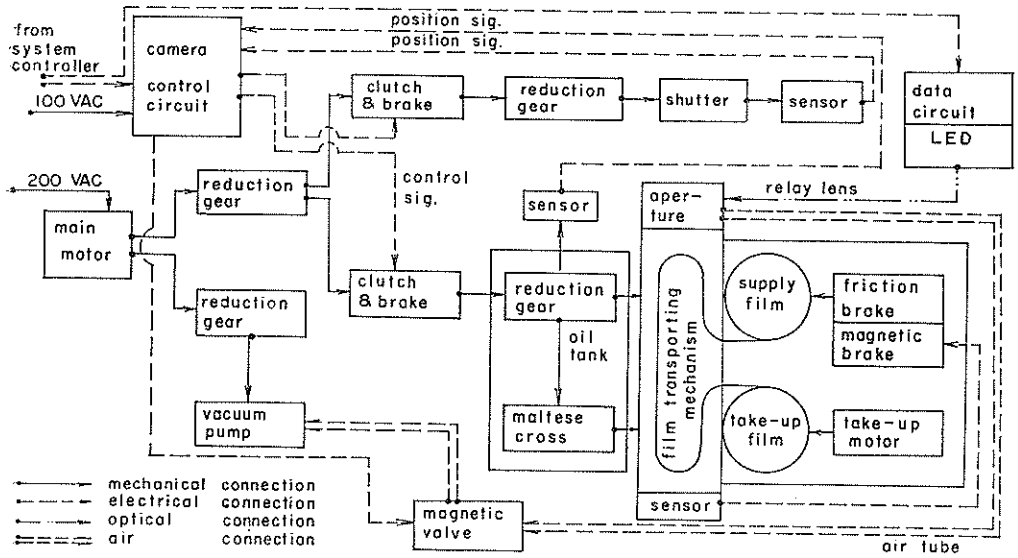

Fig. A. 7 Drive Mechanism of Pulse Data Camera

The Guide Number in the above specifications is the coefficient of exposure by the electronic flash bulb. The Guide Number (G. N.) is determined by the relation; $G.N.=L\times F$, where L is the distance between the light source and the object and F is the aperture ratio of lens. Luminous energy required for the light source corresponding to the above mentioned Guide Number is determined under the conditions of a) distance between the light source and the object, b) lens aperture ratio, c) film sensitivity, and d) transmission factor of acrylic resin of the windows. As the light ray must penetrate through three acrylic resin plates until it reaches to the film, the intensity of the light is decreased to 25 % by penetrating them four times; flash window……transparent window of specimen container……transparent window of specimen container (return) ……shooting window.

A. 3. 4 Projector

The specifications of the projector originally designed for the present system are;

a) film feeding mode : 1-10 frames auto-step forward and reverse
b) light control : available
c) film flatness : ± 0.013 mm (with the use of aperture glass plate and vacuum absorption)
d) temperature increase : within 5 degrees Celsius at all time
e) large reflecting mirror : radius of curvature, 1000 m

A. 3. 5 Digitizer

The Seiko D-SCAN was chosen for the system whose specifications are already described in A. 2. 2 (5).

A. 3. 6 Data Processor

Recording and compensation of the measured data on the digitizing board are carried

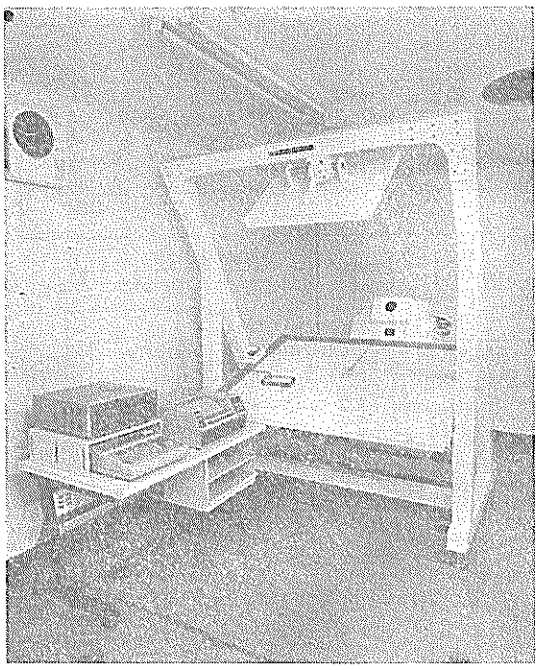

Fig. A. 8 Projector, Digitizer and Data Processor

out by the data processor consisting of a) microcomputer (HP 9825 T), b) plotter/printer (HP 7245 B), and c) interface (98034 A HP-IB). The projector, digitizer and data processor are shown in Fig. A. 8.

A. 4 Total Evaluation Test

A total evaluation test of the photo-instrumentation system has been done for the photographs taken at the window I using a test chart as an object. The test chart with 39 marks whose coordinates are already measured at the accuracy of 0.001 mm is actually put in the specimen box and is rotated up to 165 rpm. photographs are taken during flight under the same condition as the actual testing and projected onto the digitizing board to be read out. The data from the digitizer were transmitted to the microcomputer and compensated by eq. (7). Table A. 7 shows the test data where the numbers 1 to 39 denote the known marks on the test chart. In the evaluation test, the points numbered from 1 to 13 are assumed to be the fiducial points and the points numbered from 14 to 39 to be points with unknown coordinates. In the table, the exact coordinates of each point are shown in the column "on object", the measured coordinates of the each point on the digitizing board is shown in the column "observed" and the compensated coordinates of the each point is shown in the column "corrected". Error in the measurement of the coordinates of each point is shown in the column "difference".

From the evaluation test result, it is proved that the present photographic instrumentation system can measure any point on the object with the accuracy of the length less than $\pm$ 0.1 mm.

Table A. 7 Processed Data (units in mm)

No.	(on object) X :	Y :	(observed) X :	Y :				
1	0. 000	0. 000	351. 200	164. 360				
2	300. 008	−0. 013	792. 960	203. 600				
3	595. 016	0. 002	1227. 040	243. 040				
4	149. 993	119. 992	556. 320	360. 280				
5	449. 994	120. 003	998. 200	400. 240				
6	−0. 003	180. 029	327. 520	429. 280				
7	300. 000	180. 025	769. 600	468. 640				
8	595. 001	180. 022	1204. 560	508. 240				
9	149. 986	300. 000	532. 680	625. 640				
10	449. 990	300. 001	975. 160	665. 680				
11	−0. 006	359. 992	303. 560	694. 120				
12	299. 991	359. 998	746. 000	734. 480				
13	594. 978	360. 004	1181. 680	774. 160				
No.	(on object) X :	Y :	(observed) X :	Y :	(corrected) X :	Y :	(difference) X :	Y :
14	75. 000	−0. 003	461. 680	174. 080	74. 973	0. 003	0. 027	−0. 006
15	224. 996	0. 018	682. 320	193. 680	224. 822	0. 054	0. 174	−0. 072
16	375. 006	0. 007	903. 240	213. 520	374. 925	0. 049	0. 081	−0. 042
17	525. 011	0. 001	1123. 880	233. 520	524. 872	−0. 052	0. 139	0 053
18	−0. 003	60. 085	343. 080	252. 760	−0. 070	60. 121	0. 067	−0. 036
19	149. 996	60. 010	564. 200	272. 080	150. 003	59. 993	−0. 007	0. 017
20	300. 002	60. 017	785. 120	291. 840	300. 009	60. 013	0. 007	0. 004
21	450. 009	60. 024	1005. 880	311. 920	449. 939	60. 074	0. 070	−0. 050
22	595. 009	60. 016	1219. 520	331. 480	595. 029	60. 029	−0. 020	−0. 010
23	75. 002	119. 990	445. 720	350. 600	74. 972	120. 018	0. 030	−0. 028
24	224. 993	119. 993	666. 760	370. 240	224. 981	119. 987	0. 012	0. 006
25	374. 992	120. 002	887. 880	390. 200	375. 066	120. 023	−0. 074	−0. 021
26	525. 001	120. 005	1108. 880	410. 440	525. 064	120. 088	−0. 063	−0. 083
27	149. 986	180. 011	548. 440	448. 840	150. 030	180. 058	−0. 044	0. 047
28	449. 999	180. 032	990. 680	488. 680	450. 046	180. 020	−0. 047	0. 012
29	74. 989	240. 006	430. 120	527. 320	75. 104	240. 032	−0. 115	−0. 026
30	224. 994	239. 988	651. 000	547. 200	224. 928	240. 061	0. 066	−0. 073
31	374. 991	240. 002	872. 480	567. 120	375. 114	239. 992	−0. 123	0. 010
32	524. 992	239. 997	1093. 560	587. 400	524. 983	240. 079	0. 009	−0. 082
33	0. 002	300. 007	311. 520	605. 840	0. 018	300. 057	−0. 020	−0. 050
34	299. 990	299. 991	753. 920	645. 480	300. 005	299. 858	−0. 015	0. 133
35	594. 988	300. 025	1189. 320	685. 480	594. 994	300. 048	−0. 006	−0. 023
36	74. 991	359. 979	414. 120	704. 320	74. 986	360. 044	0. 005	−0. 065
37	224. 986	359. 987	635. 320	724. 360	224. 964	360. 022	0. 022	−0. 035
38	374. 985	360. 027	856. 760	744. 480	375. 017	360. 007	−0. 032	0. 020
39	524. 985	360. 011	1078. 200	764. 840	524. 968	360. 098	0. 017	−0. 087

References for Appendix A

1) Terashi, M., Ando, K., Hosoya, S. and Funasaka, T., Delopment of qualitative photo-instrumentation system by means of 70 mm data camera & analyzer, *Optical Systems Engineering III*, William H. Taylor, Editor, Proc. *SPIE 389*, 62-74, 1983.
2) Eastman Kodak Company, Kodak black and white instrumentation Film, *Kodak Publication*, No. P-92, 1971.
3) Eastman Kodak Company, High-speed Photograpgy, *Kodak Publication*, No. G-44, 22 p., 1975.
4) Watanabe, K., *Photogrammetry*, Kyoritsu Shuppan Co. Ltd., 24 p., 1976 (in Japanese).
5) Shashin Kogyo Publishing Co. Ltd., *Photographic Lens Handbook*, pp. 33-38, 1978 (in Japanese)
6) Nippon Kogaku K. K., *Lens Data Book* (in Japanese)
7) Hayashi, K. and Kuboshima, M., *Camera and Lenses*, Photographic Technical Course 1, pp. 235-237, 1957 (in Japanese)
8) Shashin Kogyo Publishing Co Ltd., *Large Format Camera*, No. 319. 20 p., 1976 (in Japanese)
9) Kubota, H., *Optics*, Iwanami Shoten Publishers, pp. 349-351, 1964 (in Japanese).